

EINDHOVEN  
UNIVERSITY OF TECHNOLOGY

MECHANICAL ENGINEERING  
BACHELOR END PROJECT

---

## Stabilization of parametrically excited pendulum

---

STABILIZATION OF PARAMETRICALLY EXCITED PENDULUM

*Authors:*

Thijs van Oorschot (1352725)

*Supervisors:*

Sasha Pogromskiy



Eindhoven, July 4, 2021

# Contents

<b>List of symbols</b>	<b>2</b>
<b>1 Introduction</b>	<b>3</b>
<b>2 Derivation of equations of motion</b>	<b>4</b>
2.1 Relevant parameters of pendulum . . . . .	4
2.2 Derivation of Lagrange equation of motion . . . . .	4
2.3 Linearizing Lagrange equation of motion . . . . .	6
<b>3 Stability analysis</b>	<b>8</b>
3.1 Simplified expression for oscillation of pivot point . . . . .	8
3.2 Model for stability analysis . . . . .	9
3.3 Influence of damping on stability . . . . .	12
<b>4 Model vs. experiment around lower equilibrium position</b>	<b>13</b>
4.1 Explanation of test setup . . . . .	13
4.2 Model vs. experiment comparison . . . . .	15
<b>5 Design of experimental setup for stabilization in upper equilibrium position</b>	<b>17</b>
5.1 General concept . . . . .	17
5.2 Details of design . . . . .	18
5.3 Design evaluation . . . . .	20
<b>6 Model v.s. experiment in upper equilibrium position</b>	<b>22</b>
6.1 Explanation of experiment . . . . .	22
6.2 Assumptions for the predicted stability regions . . . . .	22
6.3 Model vs. experiment comparison . . . . .	24
6.4 Possible causes for model inaccuracy . . . . .	26
<b>7 Conclusion</b>	<b>26</b>
<b>References</b>	<b>27</b>
<b>A Appendix: Estimation of damping coefficients</b>	<b>28</b>
A.1 Estimation of damping coefficient TU/e setup . . . . .	28
A.2 Estimation of damping coefficient self-made setup . . . . .	29
<b>B Appendix: Measurement technique with video</b>	<b>32</b>
B.1 Error of video . . . . .	32
B.2 Explanation of position extraction from video . . . . .	33
B.2.1 Frequency estimation of self-made setup . . . . .	34
B.2.2 Damping estimation of self-made setup . . . . .	35
B.2.3 Damping estimation of TU/e setup . . . . .	36
<b>C Appendix: Data sheet of DC-motor</b>	<b>37</b>
<b>D Appendix: self-made test setup images</b>	<b>38</b>
<b>E Appendix: MATLAB-scripts</b>	<b>38</b>
E.1 MALTAB-script that predicts stability . . . . .	38
E.2 MATLAB-script that reads video . . . . .	39

## List of symbols

Symbol	Variable	Unit	Unit abbreviation
$\Delta L$	Offset of pivot point	Meters	[m]
$\Delta x$	Distance from center of wheel to pivot point	Meters	[m]
$\lambda$	Eigenvector	-	[-]
$\varphi$	Angle of pendulum w.r.t. vertical	Rad	[rad]
$\psi$	Linearized angle pendulum w.r.t. vertical	Radians	[rad]
$\omega$	Angular velocity	Radians per second	[rad/s]
A	Amplitude of oscillation	Meters	[m]
a	Acceleration of pivot point	meter per second squared	[m/s <sup>2</sup> ]
b	Length of rope	Meters	[m]
b	Length of connecting rod	Meters	[m]
c	Distance from pivot point to center of mass	Meter	[m]
D	Diameter of axis	Meters	[m]
d	Viscous damping coefficient	Newton second per meter	[Ns/m]
f	Frequency	Hertz	[Hz]
G	Center of mass	Meters	[m]
g	Gravitational acceleration	Meter per second squared	[m/s <sup>2</sup> ]
$I_G$	Mass moment of inertia	Kilogram meter squared	[kgm <sup>2</sup> ]
i	Transmission ratio	-	[-]
i	Distance between camera and pendulum	Meters	[m]
j	Distance between pendulum and wall	Meters	[m]
L	Length of pendulum	Meters	[m]
m	Mass of pendulum	Kilogram	[kg]
$Q^{nc}$	Non-conservative force	Newton	[N]
r	Radius	Meters	[m]
T	Period of oscillation	Seconds	[s]
$T_{kin}$	Kinetic energy	Joule	[J]
t	Time	Seconds	[s]
u	Horizontal deflection of pendulum	Meters	[m]
V	Potential energy	Joules	[J]
V	Voltage	Volts	[V]
W	Width of pendulum	Meters	[m]
y	Vertical position of pivot point	Meters	[m]

## 1 Introduction

In engineering, it is important to evaluate the stability of structures. History has taught us that instability can cause structures to collapse. In nature, a lot of structures can be considered as a pendulum. The formal definition of a pendulum is a weight suspended to a certain pivot point. A pendulum is typically stable in the lower position (i.e. with the tip of the pendulum pointing down) and unstable in the upper position (i.e. with the tip of the pendulum pointing up). It is generally known that one can stabilize or destabilize a pendulum by moving its pivot point in the horizontal direction. For instance, one can balance a stick on his hand by moving it around. However, it is also possible to destabilize the pendulum when it is pointing down or stabilizing a pendulum when it is pointing up by oscillating its pivot point in the vertical direction. For instance, when a ship is floating on a sea with heavy waves, the vertical oscillation can cause the ship start to rotate from side to side with an increasing amplitude, until it capsizes. This phenomenon of losing stability due to periodic oscillations causing ships to capsize has been investigated before by Maki, A. et al. [1]. Similarly, in 1940 the Tacoma Narrows-bridge in the United States collapsed due to the fact that it was designed in such a way that the wind caused it to oscillate in its eigenfrequency [2]. The phenomenon of (de)stabilizing pendulums with a vertical oscillation of the pivot point is explored in this report.

The goal of this project is to design and build a simple experimental setup to stabilize a pendulum in the upper equilibrium position, i.e. when the pendulum is pointing in the upward direction. Due to the COVID-19 measurements, the facilities on the TU/e campus cannot be accessed to build a test setup. Therefore, the experimental setup should be assembled at home, with components that can be found at home or obtained easily during the pandemic. Experiments are performed with this experimental test setup and a test setup provided by the TU/e. The setup provided by the TU/e is meant to destabilize pendulums in the lower equilibrium position, i.e. when the pendulum is pointing down. Furthermore, a model should be developed that predicts the behaviour of these experiments. To this end, remote measurements are performed, using a camera, and a technique is developed to read relevant data from the video, to measure the behaviour of the pendulum.

## 2 Derivation of equations of motion

In this chapter, the equations of motion of the problem are derived. First, the relevant parameters of the pendulum are defined. Then, the non-linear Lagrange-equation is derived and linearized to get the final equations of motion.

### 2.1 Relevant parameters of pendulum

Figure 2.1 shows a schematic representation of the pendulum with length L. The angle w.r.t. the vertical is denoted by  $\phi$ . The center of mass is denoted by G, the pivot point is denoted by O, and the prescribed displacement of the pivot point is denoted by y. The distance from the pivot point to the center of mass is denoted by c. Finally, the mass and mass moment of inertia around its center of mass are denoted by m and  $I_G$  respectively.

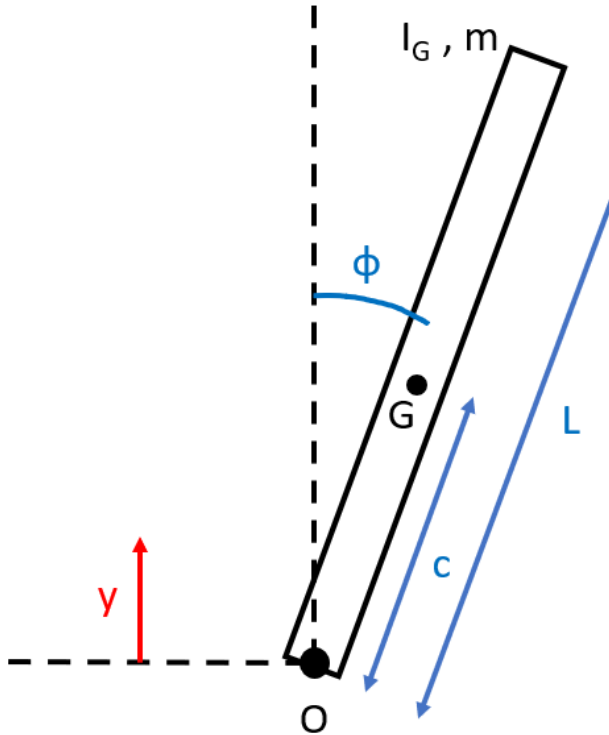


Figure 2.1: Sketch of pendulum-problem

### 2.2 Derivation of Lagrange equation of motion

In this section, the 5 steps taken to obtain the Lagrange equation of motion are elaborated.

#### Step 1: define generalized coordinates

There is only 1 generalized coordinate, denoted by q, which is the angle of the pendulum w.r.t. the vertical, as presented below. The prescribed motion is the vertical displacement of the pivot point of the pendulum, denoted by y.

$$q = \phi \quad (2.1)$$

#### Step 2: derive an expression for the kinetic energy

The total kinetic energy is the sum of the rotational and translational kinetic energy, and its expression is presented below. In this expression,  $r_G$  represents the position vector from the pivot point to the center of

mass of the pendulum.

$$T_{kin} = T_{rot} + T_{trans} = \frac{1}{2}m \cdot \dot{r}_G^T \cdot \dot{r}_G + \frac{1}{2}I_G \cdot \dot{\phi} = \frac{1}{2}m(c^2\dot{\phi}^2 + \dot{y}^2 - 2\sin(\phi) \cdot c\dot{\phi}) + \frac{1}{2} \cdot I_G \cdot \dot{\phi}^2 \quad (2.2)$$

### Step 3: derive an expression for the non-conservative forces

There is a frictional torque in the pivot point of the pendulum. It is assumed that this is a viscous damping force, meaning that its magnitude depends on the angular velocity of the pendulum. The damping coefficient of this frictional torque is denoted by  $d$ . The expression of the total non-conservative is presented below.

$$Q^{nc} = -\dot{\phi} \cdot d \quad (2.3)$$

### Step 4: : Derive an expression for the potential energy

The expression of the total potential energy of the pendulum due to gravity is presented below.

$$V = m \cdot g \cdot (y + \cos(\phi) \cdot c) \quad (2.4)$$

To find the equilibrium positions of the system, the potential energy is derived w.r.t. the generalized coordinate  $\phi$  and equated to 0. This gives us 2 equilibrium positions,  $\phi = 0$  and  $\phi = \pi$ .

$$\frac{d}{dq}(V) = -m \cdot g \cdot \sin(\phi) \cdot \rho = 0 \rightarrow \phi = 0 \cup \phi = \pi \quad (2.5)$$

The 2 equations below show that  $\phi = 0$  is the unstable equilibrium position and that  $\phi = \pi$  is the stable equilibrium position.

$$\frac{d^2}{dq^2}(V) |_{q=0} = -m \cdot g \cdot \rho < 0 \quad (2.6) \quad \frac{d^2}{dq^2}(V) |_{q=\pi} = m \cdot g \cdot \rho > 0 \quad (2.7)$$

### Step 5: Apply Lagrange's equation of motion

The expression for Lagrange's equation of motion is presented below.

$$\frac{d}{dt}T_{,\dot{q}} - T_{,q} + V_{,q} = Q^{nc} \quad (2.8)$$

First, the 4 terms of this Lagrange equation are determined.

$$T_{,\dot{q}} = mc^2\dot{\phi} - m \cdot \dot{y} \cdot c \cdot \sin(\phi) + I_G\dot{\phi} \quad (2.9)$$

$$\frac{d}{dt}T_{,\dot{q}} = mc^2\ddot{\phi} - mc \cdot \ddot{y} \cdot \sin(\phi) - mc \cdot \dot{y} \cdot \dot{\phi} \cdot \cos(\phi) + I_G\ddot{\phi} \quad (2.10)$$

$$T_{,q} = -mc \cdot \dot{y} \cdot \cos(\phi)\dot{\phi} \quad (2.11)$$

$$V_{,q} = -mgc \cdot \sin(\phi) \quad (2.12)$$

These 4 terms are then filled into Equation 2.8 and the equation is simplified. The resulting Lagrange differential equation is presented below. This is a non-linear differential equation due to the  $\sin(\phi)$  term.

$$(mc^2 + I_G) \cdot \ddot{\phi} - m \cdot c \cdot (\ddot{y} + g) \cdot \sin(\phi) = -\dot{\phi} \cdot d \quad (2.13)$$

### 2.3 Linearizing Lagrange equation of motion

In order to analyze the stability of the pendulum, the Lagrange equation needs to be linearized. Therefore, vector  $\bar{z}$  is introduced.

$$\bar{z} = \begin{bmatrix} z_1 \\ z_2 \end{bmatrix} = \begin{bmatrix} \phi \\ \dot{\phi} \end{bmatrix} \quad (2.14)$$

This vector is applied to Equation 2.13, and the resulting state-space is given below.

$$\begin{aligned} \dot{z}_1 &= \dot{\phi} \\ \dot{z}_2 &= \frac{mc(g+\ddot{s})\sin(\phi)-d\dot{\phi}}{mc^2+I_G} \end{aligned} \quad (2.15)$$

By introducing the new variable  $\xi$  and linearizing around a certain equilibrium position, the non-linear differential equation is written into a system of 2 linear differential equations, as shown below. In this system of equations,  $\xi_1$  can be considered as the linearized parameter of  $\phi$  and  $\xi_2$  can be considered as the linearized parameter of  $\dot{\phi}$ . Matrix  $\mathbb{A}$  defines the relationship between these parameters and is dependent on the system parameters. As the pivot point of the pendulum is oscillating, Matrix  $\mathbb{A}$  is time-dependent. The expression for the different elements of this matrix is given below.

$$\begin{bmatrix} \dot{\xi}_1 \\ \dot{\xi}_2 \end{bmatrix} = \mathbb{A} \cdot \begin{bmatrix} \xi_1 \\ \xi_2 \end{bmatrix} \quad \text{with} \quad \mathbb{A} = \begin{bmatrix} \frac{\partial \dot{z}_1}{\partial z_1} & \frac{\partial \dot{z}_1}{\partial z_2} \\ \frac{\partial \dot{z}_2}{\partial z_1} & \frac{\partial \dot{z}_2}{\partial z_2} \end{bmatrix} \quad (2.16)$$

#### Linearization around lower equilibrium position

First, the elements of matrix  $\mathbb{A}$  are determined when the system is linearized around the lower equilibrium position, i.e. around  $\phi = \pi$ .

$$\left[ \frac{\partial}{\partial z_1} (\dot{z}_1) \right]_{\phi=\pi} = 0 \quad (2.17) \quad \left[ \frac{\partial}{\partial z_2} (\dot{z}_1) \right]_{\phi=\pi} = 1 \quad (2.18)$$

$$\left[ \frac{\partial}{\partial z_1} (\dot{z}_2) \right]_{\phi=\pi} = -\frac{m \cdot \rho(\ddot{y} + g)}{m\rho^2 + I_G} \quad (2.19) \quad \left[ \frac{\partial}{\partial z_2} (\dot{z}_2) \right]_{\phi=\pi} = \frac{-d}{m\rho^2 + I_g} \quad (2.20)$$

$$\mathbb{A} = \begin{bmatrix} 0 & 1 \\ -\frac{m \cdot \rho(\ddot{y} + g)}{m\rho^2 + I_G} & \frac{-d}{m\rho^2 + I_g} \end{bmatrix} \quad (2.21)$$

### Linearization around upper equilibrium position

Then, the elements of matrix  $\mathbb{A}$  are determined when the system is linearized around the upper equilibrium position, i.e. around  $\phi = 0$ .

$$\left[ \frac{\partial}{\partial z_1} (\dot{z}_1) \right]_{\phi=0} = 0 \quad (2.22) \quad \left[ \frac{\partial}{\partial z_2} (\dot{z}_1) \right]_{\phi=0} = 1 \quad (2.23)$$

$$\left[ \frac{\partial}{\partial z_1} (\dot{z}_2) \right]_{\phi=0} = \frac{m \cdot c(\ddot{y} + g)}{mc^2 + I_g} \quad (2.24) \quad \left[ \frac{\partial}{\partial z_2} (\dot{z}_2) \right]_{\phi=0} = \frac{-d}{mc^2 + I_g} \quad (2.25)$$

$$\mathbb{A} = \begin{bmatrix} 0 & 1 \\ \frac{m \cdot \rho(\ddot{y} + g)}{m\rho^2 + I_g} & \frac{-d}{m\rho^2 + I_g} \end{bmatrix} \quad (2.26)$$

It is interesting to note that the only difference between the matrix  $\mathbb{A}$  of the upper and the lower equilibrium position is the sign in front of the bottom left element.

Matrix  $\mathbb{A}$  depends on the second time derivative of the horizontal position of the pivot point, which is generally a function of time. Therefore, matrix  $\mathbb{A}$  is also a function of time. This complicates the stability analysis of the system. This problem is solved in section 3.1.

### 3 Stability analysis

In chapter 2, the equations of motions of the pendulum are derived. In this chapter, the stability of these equations is evaluated. First, the method of computing the stability of the pendulum is explained. To this end, an expression for the oscillation profile of the pivot point is derived. Then, an exemplary stability plot is presented to get an idea of the influence of the distance from the pivot point to the center of mass ( $c$ ) and the excitation frequency ( $f$ ) on the stability regions. Finally, the influence of the viscous damping coefficient ( $d$ ) is evaluated.

#### 3.1 Simplified expression for oscillation of pivot point

The acceleration of the pivot point depends on the design of the setup. However, for the stability computations, it is assumed that the excitation of the base of the pendulum happens at a constant acceleration  $\ddot{y}$ . Therefore, the y-position of the pivot-point of the pendulum as a function of time is a second-order polynomial function. As the y-position should be an oscillating profile, the sign of the acceleration  $\ddot{y}$  switches sign at every half of the period. The amplitude of the oscillation is denoted by  $A$ , and its frequency is denoted by  $f$ , called the excitation frequency. Therefore, the period of the oscillation is  $T = \frac{1}{f}$ . Equation 3.1 presents the assumed position of the pivot point as a function of time, and Equation 3.2 presents the assumed acceleration of the pivot point as a function of time. Clearly, the y-position is a second-order polynomial, and the acceleration does not depend on time.

$$y = \begin{cases} y_1(t) = -\frac{16 \cdot A}{T^2} \cdot t^2 + A & \text{if } t \in [\frac{(k-1)T}{2}, \frac{kT}{2}) \\ y_2(t) = \frac{16 \cdot A}{T^2} \cdot t^2 - A & \text{if } t \in [\frac{kT}{2}, \frac{(k+1)T}{2}) \end{cases} \quad \text{for } k = 1, 2, 3, \dots \quad (3.1)$$

$$a = \begin{cases} a_1(t) = a_1 = -\frac{32 \cdot A}{T^2} & \text{if } t \in [\frac{(k-1)T}{2}, \frac{kT}{2}) \\ a_2(t) = a_1 = \frac{32 \cdot A}{T^2} & \text{if } t \in [\frac{kT}{2}, \frac{(k+1)T}{2}) \end{cases} \quad \text{for } k = 1, 2, 3, \dots \quad (3.2)$$

To get an idea of this assumed excitation oscillation, the y-position and y-acceleration of the pivot point are plotted for a frequency  $f = 5$  [Hz] and amplitude  $A = 5$  [cm].

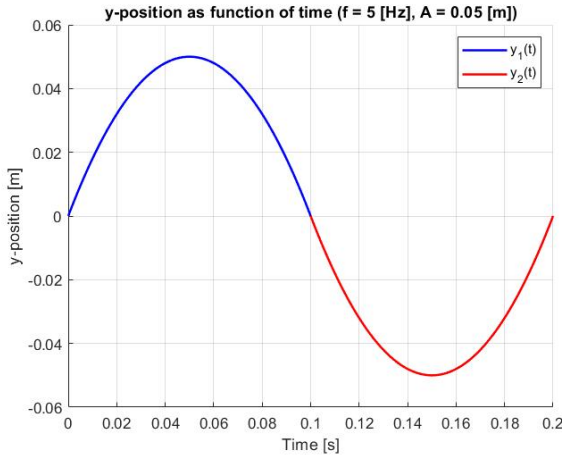


Figure 3.1: Simplified excitation oscillation position as a function of time with frequency  $f = 5$  [Hz] and amplitude  $A = 5$  [cm]

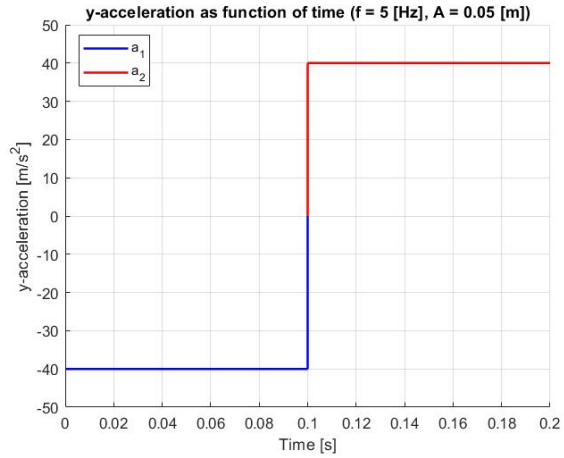


Figure 3.2: Simplified excitation oscillation acceleration as a function of time with frequency  $f = 5$  [Hz] and amplitude  $A = 5$  [cm]

The advantage of using this oscillation profile is that the second order time derivative of  $y$  is constant. This means that matrix  $\mathbb{A}$  becomes a piecewise function of time, i.e. 2 matrices are defined, and the system

switches between these 2 matrices at every half period.

### 3.2 Model for stability analysis

The problem is considered to be a time-dependent bi-modal switching system. The system is bi-modal because it has 2 modes, one with a positive acceleration  $a_1$  and one with a negative acceleration  $a_2$ . The system is time-dependent because it switches between the 2 modes at fixed times. The expression below shows the switching system in the case of this pendulum [3].

$$\dot{\xi} = \mathbb{A}_{i(t)}\bar{\xi}, \quad \begin{cases} i = 1 & \text{if } t \in [\frac{(k-1)T}{2}, \frac{kT}{2}) \\ i = 2 & \text{if } t \in [\frac{kT}{2}, \frac{(k+1)T}{2}) \end{cases} \quad \begin{matrix} \text{mode 1} \\ \text{mode 2} \end{matrix} \quad k = 1, 2, 3, \dots \quad (3.3)$$

The solutions by the end of the switching intervals can be calculated. Equation 3.4 and Equation 3.5 show the solution after 1 and 2 switches respectively.

$$\xi\left(\frac{T}{2}\right) = e^{\frac{T}{2}A_1} \cdot \xi_0 \quad (3.4) \quad \xi(T) = e^{\frac{T}{2}A_2} \cdot \xi\left(\frac{T}{2}\right) = e^{\frac{T}{2}A_2} \cdot e^{\frac{T}{2}A_1} \cdot \xi_0 \quad (3.5)$$

Equation 3.6 shows the general solution after  $k$  periods of oscillation of the pivot point. As  $k \rightarrow \infty$ , matrix  $\mathbb{M}$  determines whether the solution diverges or converges. If the solution converges, the system is stable. This is the case when matrix  $\mathbb{M}$  has eigenvalues in the open disc unit (a circle with radius 1), i.e. when the length of the eigenvalues is smaller than 1 [4]. This condition is depicted in Equation 3.7 and is called the Schur-condition, i.e. when this condition is satisfied, the system is stable and the angle of the pendulum will converge to its equilibrium position.

$$\xi(kT) = [e^{\frac{T}{2}A_2} \cdot e^{\frac{T}{2}A_2}]^k \cdot \xi_0 = \mathbb{M}^k \cdot \xi_0 \quad \text{with} \quad \mathbb{M} = e^{\frac{T}{2}A_2} \cdot e^{\frac{T}{2}A_2} \quad (3.6)$$

$$\sqrt{\operatorname{Re}(\lambda_i)^2 + \operatorname{Im}(\lambda_i)^2} < 1 \quad (3.7)$$

Matrix  $\mathbb{M}$  contains exponents of matrices  $\mathbb{A}_1$  and  $\mathbb{A}_2$ . This can be calculated analytically using Taylor-expansions. In MATLAB, this can be calculated using the command **expm()**.

To analyse the stability of the parametrically excited pendulum, the 3 parameters  $\varepsilon$ ,  $\omega$  and  $\beta$  are defined.  $\varepsilon$  contains the acceleration of the pivot point.  $\omega$  represents the natural frequency of the pendulum.  $\beta$  contains the friction coefficient in the pivot point of the pendulum.

$$\varepsilon = \frac{m \cdot c \cdot \ddot{y}}{mc^2 + I_G} \quad (3.8) \quad \omega^2 = \frac{m \cdot c \cdot g}{mc^2 + I_G} \quad (3.9) \quad \beta = \frac{d}{mc^2 + I_G} \quad (3.10)$$

#### Stability analysis in lower equilibrium position

Equation 3.11 and Equation 3.12 show matrix  $\mathbb{A}_1$  and  $\mathbb{A}_2$  respectively for when the pendulum is in the lower equilibrium position.  $\mathbb{A}_1$  represents the system with a positive acceleration and  $\mathbb{A}_2$  represents the system with a negative acceleration.

$$\mathbb{A}_1 = \begin{bmatrix} 0 & 1 \\ -\epsilon - \omega^2 & -\beta \end{bmatrix} \quad (3.11) \quad \mathbb{A}_2 = \begin{bmatrix} 0 & 1 \\ \epsilon - \omega^2 & -\beta \end{bmatrix} \quad (3.12)$$

To analyse the stability of the pendulum around the lower equilibrium position, the eigenvectors of matrix  $\mathbb{M}$  are determined for varying values of the distance from the pivot point to the center of mass  $c$  and varying values of the excitation frequency  $f$ . As an example, the length of the 2 eigenvectors are plotted as a function of these 2 parameters below, for arbitrary system parameters  $m = 1 \text{ [kg]}$ ,  $I_G = 0.1 \text{ [kgm}^2]$ ,  $d = 0.02 \text{ [Ns/m]}$  and  $A = 5 \text{ [cm]}$ .

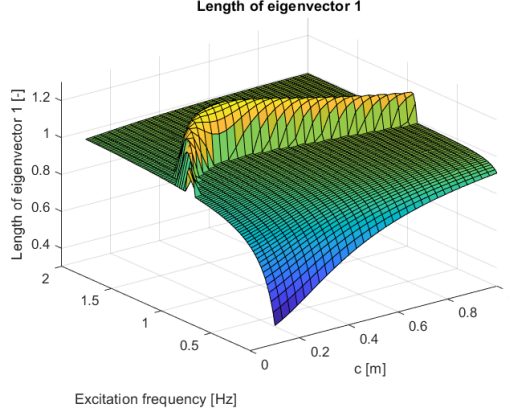


Figure 3.3: Length of eigenvector 1

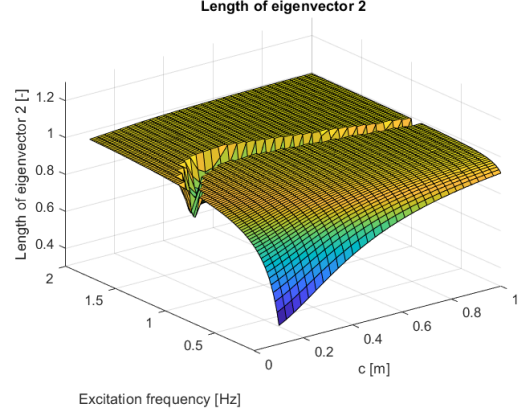


Figure 3.4: Length of eigenvector 2

As explained, the system is stable, i.e. converges to its equilibrium position, when the length of both these eigenvectors are smaller than 1. This is verified for each combination of  $c$  and  $f$ . The result is plotted in the figure below. Black regions represent unstable combinations of  $c$  and  $f$ , and white regions represent stable combinations. The MATLAB-script that is used to compute this stability figure is presented in subsection E.1. This figure provides an idea of the influence of the distance  $c$  and excitation frequency  $f$  on the stability around the lower equilibrium position.

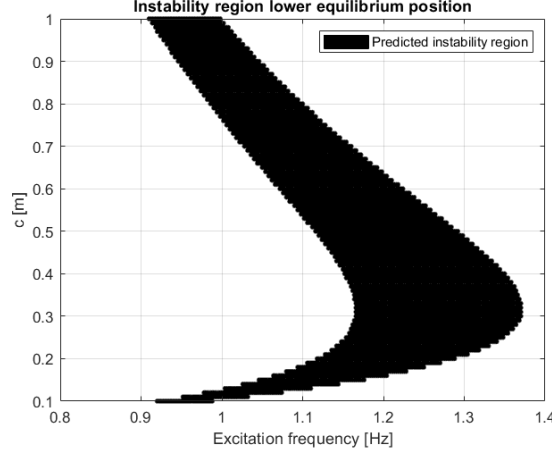


Figure 3.5: Instability region around lower equilibrium position.  $m = 1 \text{ [kg]}$ ,  $I_G = 0.1 \text{ [kgm}^2]$ ,  $d = 0.02 \text{ [Ns/m]}$ ,  $A = 5 \text{ [cm]}$

### Stability analysis in upper equilibrium position

Equation 3.13 and Equation 3.14 show matrix  $\mathbb{A}_1$  and  $\mathbb{A}_2$  respectively for when the pendulum is in the upper equilibrium position.  $\mathbb{A}_1$  represents the system with a positive acceleration and  $\mathbb{A}_2$  represents the system with a negative acceleration.

$$\mathbb{A}_1 = \begin{bmatrix} 0 & 1 \\ -\epsilon + \omega^2 & -\beta \end{bmatrix} \quad (3.13) \quad \mathbb{A}_2 = \begin{bmatrix} 0 & 1 \\ \epsilon + \omega^2 & -\beta \end{bmatrix} \quad (3.14)$$

Again, as an example, the length of the eigenvectors are determined for varying values of distance  $c$  and excitation frequency  $f$ . This is done for arbitrary system parameters  $m = 1$  [kg],  $I_G = 0.01$  [kgm<sup>2</sup>],  $d = 0.1$  [Ns/m] and  $A = 5$  [cm]. The result is plotted in the figures below.

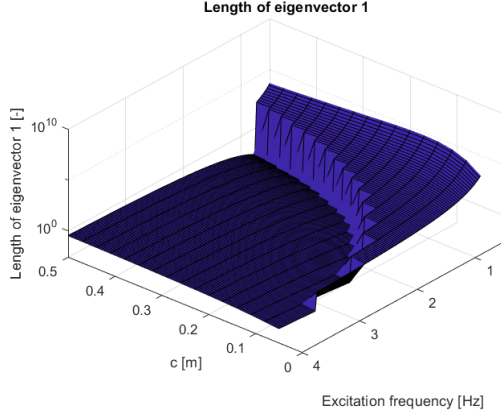


Figure 3.6: Length of eigenvector 1

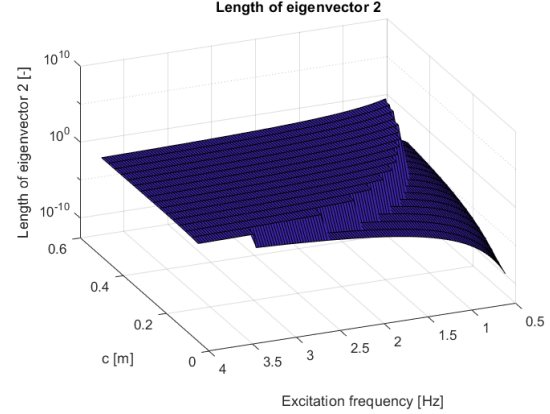


Figure 3.7: Length of eigenvector 2

It is interesting to note that, in the unstable regions, the order of magnitude of the eigenvectors of the system linearized around the upper equilibrium position is much larger than the order of magnitude of the eigenvectors of the system linearized around the lower equilibrium position. This means that the system is more unstable in its upper equilibrium position than the system in its lower equilibrium position, i.e. when unstable, the pendulum with diverge away from its equilibrium position more quickly in the upper position than in the lower position.

Using the lengths of the eigenvectors, a stability plot is created as presented below. Black regions represent unstable combinations of  $c$  and  $f$ , white regions represent stable combinations. The MATLAB-script that is used to compute this stability figure is presented in subsection E.1. Again, the figure provides an idea of the influence of the distance  $c$  and excitation frequency  $f$  on the stability, this time around the upper equilibrium position.

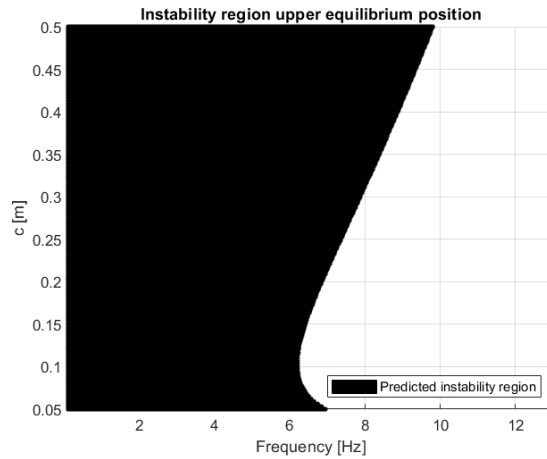


Figure 3.8: Instability region around upper equilibrium position.  $m = 1$  [kg],  $I_G = 0.01$  [kgm<sup>2</sup>],  $d = 0.1$  [Ns/m],  $A = 5$  [cm]

### 3.3 Influence of damping on stability

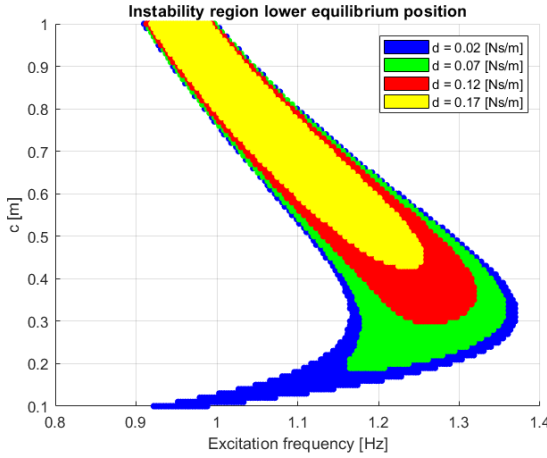


Figure 3.9: Instability regions for different damping coefficients around lower equilibrium position

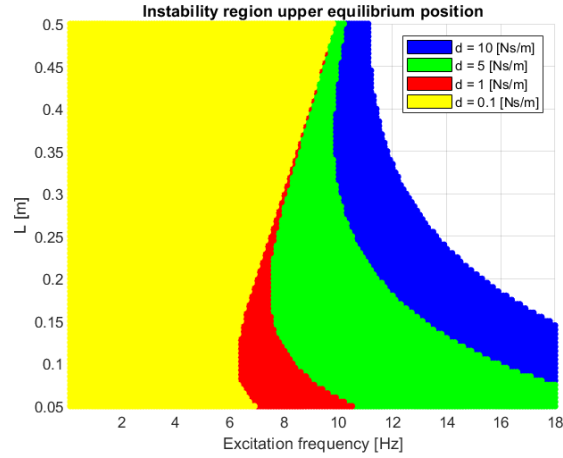


Figure 3.10: Instability regions for different damping coefficients around upper equilibrium position

To get an idea of the influence of the viscous damping coefficient on the stability of the pendulum, the instability regions are plotted for varying values of this damping coefficient in the figures above, both for the lower and upper equilibrium position. Note that instability regions are placed on top of each other. This means that the blue instability region continues underneath the other 3 instability regions, the green instability region continues underneath the red and yellow instability regions, and the red instability region continues underneath the yellow instability region.

Figure 3.9 shows that the instability of the lower equilibrium position region shifts upwards and its surface area decreases for an increasing damping coefficient. This means that for pendulums with a relatively high damping coefficient, a higher excitation frequency is required to destabilize the pendulum. This influence of the damping coefficient becomes smaller for a longer distance  $c$ . Furthermore, for higher damping coefficients, the minimum distance  $c$  required in order to destabilize the pendulum is increased. In conclusion, a high damping coefficient has a stabilizing effect on the pendulum around its lower equilibrium position, i.e. it is easier to destabilize a pendulum with low damping in its pivot point.

Figure 3.10 shows that the surface area of the instability region of the upper equilibrium position is increased for an increasing damping coefficient. This means pendulums with a relatively high damping coefficient require a higher excitation frequency in order to get out of the instability zone, i.e. in order to be stabilized. This influence of the damping coefficient becomes smaller for a longer distance  $c$ . In conclusion, a high damping coefficient has a destabilizing effect on the pendulum around its upper equilibrium position, i.e. it is easier to stabilize pendulums with a low damping coefficient.

## 4 Model vs. experiment around lower equilibrium position

In this chapter, the model that computes the stability regions for the lower equilibrium position of the pendulum is validated. This is done with a test setup provided by the TU/e. First, this test setup and its imperfections w.r.t. the assumptions of the model are elaborated. Then, the experimental results are compared with the predictions of the model to analyze its accuracy.

### 4.1 Explanation of test setup

The figure below shows a schematic representation of the test setup used to validate the lower equilibrium position stability regions. The pivot point of the pendulum does not oscillate. Instead, this oscillation is simulated by varying the length  $L$  of the pendulum. This is done by rotating the wheel with radius  $r$  with a constant angular velocity  $\omega$ . The wheel and mass  $m$  are connected by a rope. This means that the length of the pendulum varies between  $[L_0 - r, L_0 + r]$ , where  $L_0$  is the mean length of the pendulum. The use of a rope has 2 things as a consequence. Firstly, the maximum acceleration of the mass in downwards direction is  $g = 9.81[m/s^2]$ , as the rope can only bear tensile stresses. Secondly, as the mass of the rope is negligible w.r.t. the suspended mass, the mass of the pendulum is independent of the length of the pendulum. Furthermore, mass  $m$  is considered to be a point mass, meaning that the mass moment of inertia  $I_G$  of the suspended mass around its c.o.m. is assumed to be 0. The damping constant of the pivot point of the pendulum is determined experimentally to be  $d = 0.0022[Ns/m]$ . The method used to estimate this damping coefficient is presented in Appendix A. Mass  $m$  is equal to 0.124 [kg], and radius  $r$  is 5.0 [cm].

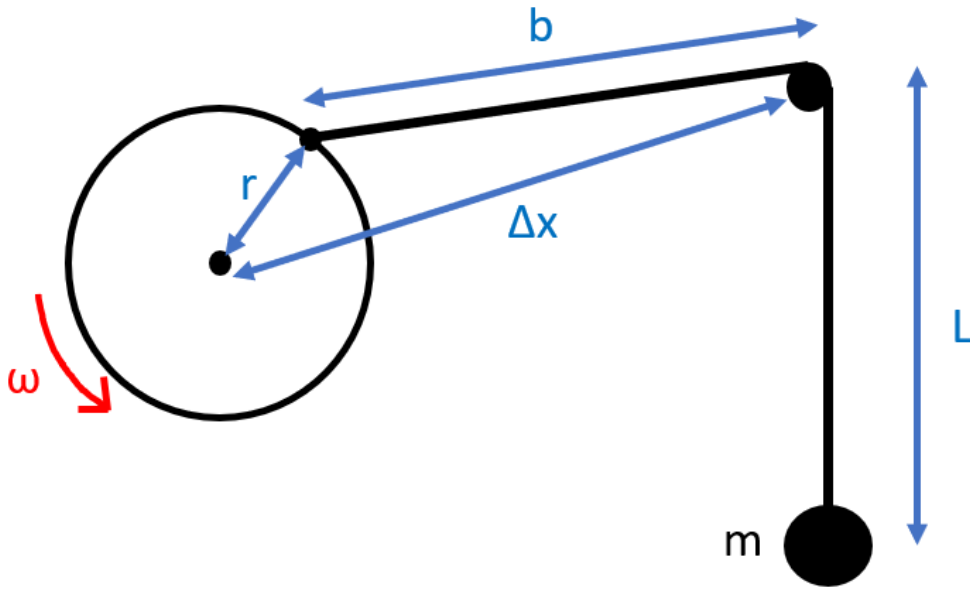


Figure 4.1: Sketch of the test setup provided by the TU/e

The expression for distance  $b$  is given in Equation 4.1. The virtual acceleration of the pivot point is assumed to be equal to the second derivative of distance  $d$  w.r.t. time, depicted in Equation 4.2.

$$b(t) = \sqrt{(\Delta x - \cos(\omega \cdot t) \cdot r)^2 + (\sin(\omega \cdot t) \cdot r)^2} \quad (4.1) \quad a(t) = \frac{d^2 b}{dt^2} \quad (4.2)$$

To evaluate the validity of this assumption, the virtual position and acceleration of the oscillation are plotted as a function of time and compared to the simplified oscillation with constant acceleration used in the stability model in Figure 4.2 and Figure 4.3 respectively. These figures show that the oscillation profiles are indeed very similar.

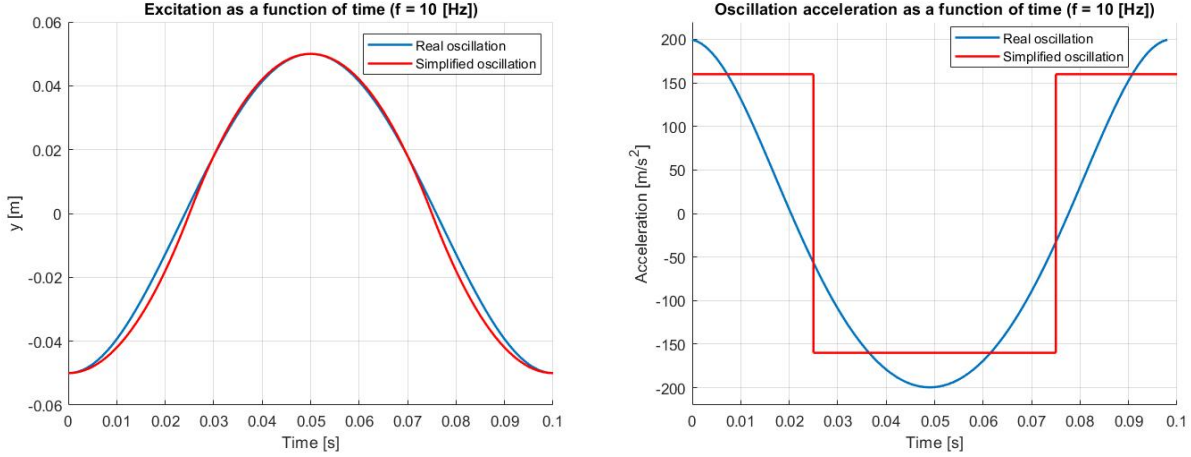


Figure 4.2: Comparison of real and simplified oscillation profile ( $f = 10$  [Hz])

Figure 4.3: Comparison of real and simplified oscillation acceleration profile ( $f = 10$  [Hz])

The angular velocity of the wheel is varied by changing the applied voltage to the driving motor. Therefore, the relation between the applied Voltage and the resulting frequency of the oscillation is determined. This is done by measuring the frequency of the oscillation for different Voltages. A second-order polynomial function is fitted through the resulted data. The measured data together with the fitted second order polynomial is plotted in Figure 4.4. The resulting expression of this polynomial is given in Equation 4.3, which gives us the relation between the applied Voltage to the motor and the angular velocity of the wheel, which is used to determine the excitation frequency.

$$f(V) = 0.002284 \cdot f^2 + 0.1412 \cdot f - 0.03152 \quad (4.3)$$

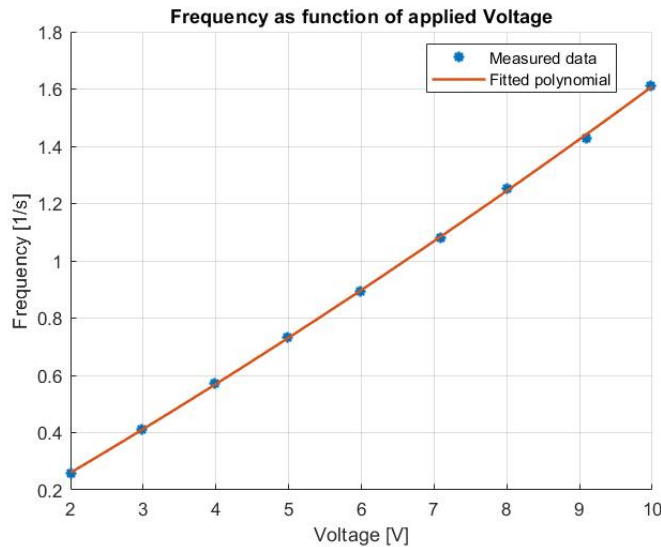


Figure 4.4: Excitation frequency as a function of the applied Voltage

## 4.2 Model vs. experiment comparison

Even though the length of the pendulum in this test-setup is not constant, this length is assumed to be constant and equal to its mean length  $L_0 = \frac{L_{min}+L_{max}}{2}$ . The Lagrangian differential equation is applied to this test setup, and it is assumed that  $c = L_0$  and  $I_G = 0$ . The resulting expression of the Lagrange differential equation is presented below.

$$mL_0^2 \cdot \ddot{\phi} - mL_0g \cdot \sin(\phi) = -d \cdot \dot{\phi} \quad (4.4)$$

This means that the system parameters  $\varepsilon$ ,  $\omega$  and  $\beta$  are simplified:

$$\varepsilon = \frac{\ddot{y}}{L_0} \quad (4.5) \quad \omega^2 = \frac{g}{L_0} \quad (4.6) \quad \beta = \frac{d}{mL_0^2} \quad (4.7)$$

Figure 4.5 and Figure 4.6 show the length of the eigenvectors as a function of the length  $L_0$  and excitation frequency  $f$ , used to predict the stability of the system. Figure 4.7 shows the predicted instability region, computed by the numerical model, as a function of the length of the pendulum  $L$  and frequency of the oscillation  $f$  (the excitation frequency). It is noticed that if the eigenfrequency is multiplied by 2 and plotted as a function of the length of the pendulum, this line goes through the middle of this instability region. It is therefore concluded that the eigenfrequency has a high influence on the instability region of the pendulum around its lower equilibrium position. This instability region is compared to the measured instability region to validate the model. To this end, the mean length of the pendulum of the test setup is measured. For this length, the applied Voltage to the motor is increased slowly, and therefore also the frequency of oscillation is increased. For certain Voltages, the pendulum becomes unstable. In this case, the pendulum starts to oscillate around its lower equilibrium position with an increasing amplitude over time. This phenomenon can be observed by eye, as after some time, the amplitude becomes relatively high. The regions where this happens are documented, and the procedure is repeated for different mean lengths of the pendulum. The results are presented in the table below and they are visualized in Figure 4.7.

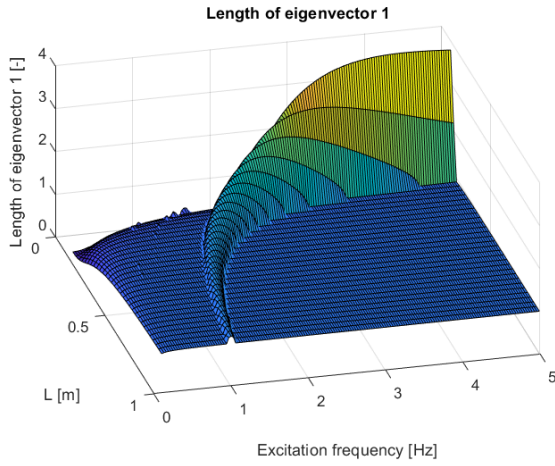


Figure 4.5: Length of eigenvector 1

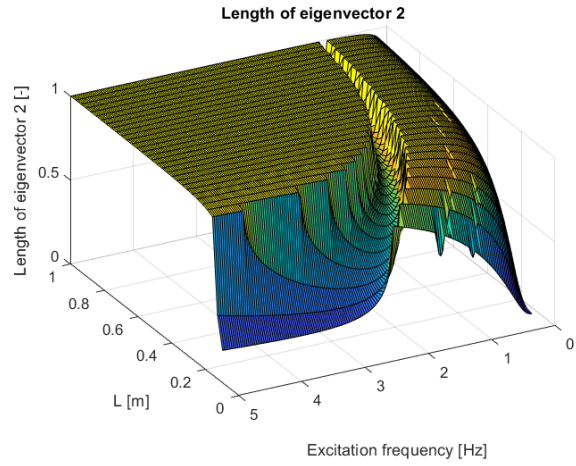


Figure 4.6: Length of eigenvector 2

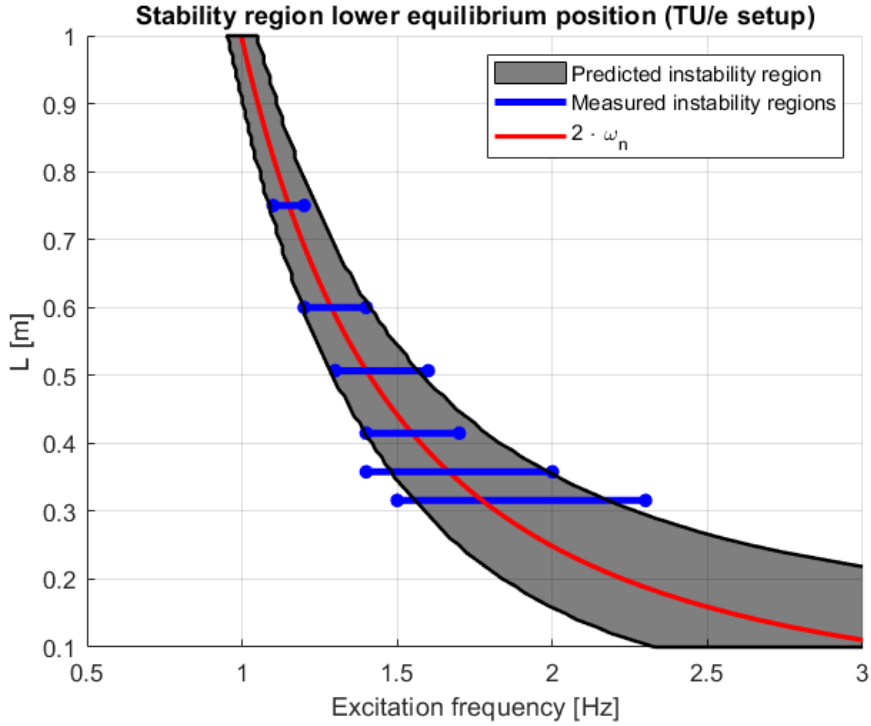


Figure 4.7: Comparison of predicted and measured instability regions around lower equilibrium position

Mean length $L_0$ [cm]	Predicted instability region [Hz]	Measured instability region [Hz]
31.6	1.55 - 2.16	1.5 - 2.3
35.8	1.48 - 1.98	1.4 - 2.0
41.5	1.39 - 1.79	1.4 - 1.7
50.7	1.28 - 1.57	1.3 - 1.6
60.0	1.19 - 1.42	1.2 - 1.4
75.0	1.08 - 1.24	1.1 - 1.2

Table 4.1: Comparison of predicted and measured instability regions around lower equilibrium position

It is observed that the model predicts the behaviour of the experiment relatively well. For short pendulums, the excitation frequency required to destabilize the pendulum is relatively high. However, the range of frequencies for which the pendulum is destabilized is relatively large. For Longer pendulums, the required excitation frequency to destabilize the pendulum decreases, but the range for which the pendulum is destabilized becomes smaller too. Furthermore, the results show that the model becomes more accurate for an increasing length. This can be explained by the fact that the assumption of a constant length holds best for pendulums with a longer length  $L_0$ . It is concluded that the model is accurate enough to predict the instability regions of the pendulum within the used range of length and excitation frequency.

## 5 Design of experimental setup for stabilization in upper equilibrium position

In this section, the design that stabilizes the pendulum in its upper equilibrium position is elaborated. First, the main requirements and the general mechanism are elaborated. Then, it is explained how this concept is carried out in practice. Finally, its differences w.r.t. the stability model are evaluated.

### 5.1 General concept

The main objective of the design is to oscillate the pivot point of the pendulum in vertical direction, in order to stabilize the pendulum around its upper equilibrium position. To this end, the motion of the pivot point should be as smooth as possible. Furthermore, the design should be relatively simple, because it should be assembled at home, as the TU/e facilities are unavailable due to the COVID-19 measurements. Finally, it should also be robust, meaning it should be as stiff and lightweight as possible. This way, the eigenfrequency of the setup will be relatively high, meaning that any vibrations of the setup are minimized.

The pendulum is attached to the so-called pendulum-base. To oscillate this pendulum-base, a crank-connecting rod mechanism is used. In this mechanism, a flywheel and the pendulum-base are connected by a connecting rod. The flywheel attached to a crankshaft that is rotated by a DC-motor. This general concept is presented below.

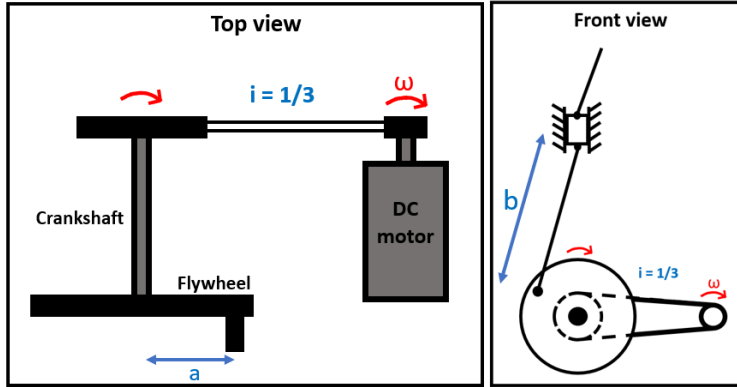


Figure 5.1: Schematic visualization of the experimental test setup to validate stability regions around the upper equilibrium position

Most DC-motors have an RPM that is higher than required to stabilize the pendulums used in this experiment. Therefore, the axis of the DC-motor is not directly attached to the crankshaft. Instead, they are connected by a driving belt. To determine the gear ratio between the driving axis of the DC-motor and the crankshaft, the predicted stability region are plotted as a function of the excitation frequency and length of the pendulum in the figure below. This gives an estimation of what excitation frequencies are required to stabilize the pendulum around its upper equilibrium position. The figure shows that excitation frequencies in the range of approximately 5 to 25 [Hz] are required. Based on this estimation, transmission ration  $i = \frac{1}{3}$  is chosen. This means that the angular velocity of the crankshaft is decreased to  $\frac{1}{3}$  of the angular velocity of the axis of the DC-motor. The angular velocity of the DC-motor can be varied using a motor driver, directed by an Arduino UNO. The value of  $a = 45$  [mm] is the distance from the center of the flywheel to the point where the connecting rod is attached, and therefore represents the amplitude of oscillation. The length of the connecting rod is denoted by  $b = 300$  [mm].

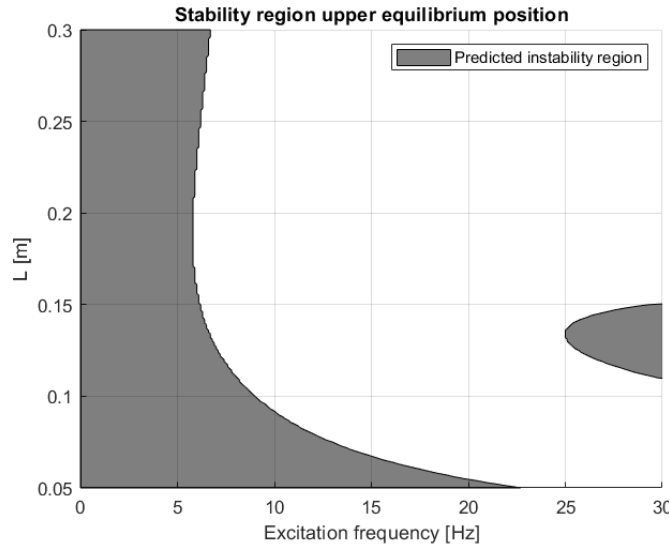


Figure 5.2: Predicted instability region

Aside from decreasing the excitation frequency, the gear connection also has another purpose. The base of the pendulum has a certain weight. Due to gravity, the pendulum will always have a force downwards. This means that the motion of the base of the pendulum upwards will not be exactly the same as the motion downwards. The gear ratio between the axis of the DC-motor and the crankshaft increases the torque that is applied to the crankshaft. Therefore, the difference between the motion of the base of the pendulum upwards and downwards is minimized.

## 5.2 Details of design

The DC-motor that is used in this test-setup is the GR 63x25 (Dunkermotoren) [5]. The datasheet of this DC-motor is presented in Appendix C. The motor is fixed in a 3D-printed motor-case. A 20-teeth pulley is attached to the driving axis of the motor. A driving belt connects this pulley to a 60-teeth pulley, which is attached to the 8mm-diameter steel driveshaft. The driveshaft can only rotate w.r.t. its longitudinal axis due to 2 ball bearings. These 2 ball bearings and the motor are fixed to the lower plate of the setup. The flywheel consists of a 15mm-thick wooden disk, clamped in between 2 pulleys that fix the disk to the crankshaft, ensuring that the disk cannot rotate w.r.t. the driveshaft. At a distance of 45 [mm] from the center of the disk, another 8mm-diameter steel axis is attached to the flywheel. Using a ball bearing, a connecting-rod connects this axis to the pendulum-base. Both the connecting rod and the pendulum-base are 3D-printed. The pendulum-base can translate over 2 8mm-diameter steel axes that are fixed to the top plate. The top and bottom plate are connected by 4 corner beams of 70x70 [mm]. The 2 plates and the 4 beams are made of wood. Figure 5.3 shows a Siemens NX-model of the final design. Figure 5.4 and Figure 5.5 show the same model, zoomed in on the pulley-mechanism with, where the 4 corner-beams are removed to improve visibility. An image of the pulley system of the real-life setup is presented in Appendix D.

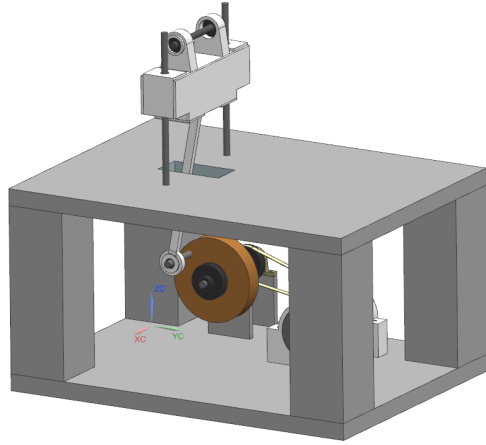


Figure 5.3: Visualization of experimental test setup

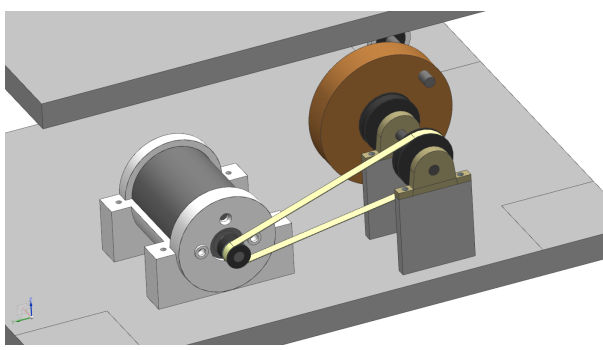


Figure 5.4: Visualization of experimental test setup , without 4 corner beams, zoomed in on pulley connection

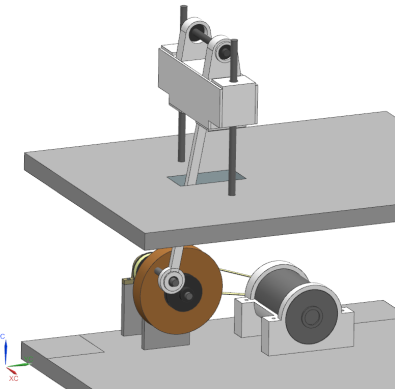


Figure 5.5: Visualization of experimental test setup, without 4 corner beams, zoomed in on crankshaft connection

The white part in Figure 5.6 and Figure 5.7 represent the 3D-printed part of the pendulum-base. 2 linear ball bearings are attached to each end of the base. These ball-bearings make sure the base can slide over the 2 guiding axes smoothly. The connecting rod is attached to the 8mm-diameter steel axis on the bottom of the base using a ball bearing. On top of the base, another 8m-diameter axis is attached to the base using 2 ball bearings. The aluminum pendulum is attached rigidly to this axis, as it is clamped in between 2 20-teeth pulleys, similarly to how the flywheel is attached to the crankshaft. This means that the pendulum cannot rotate w.r.t. this axis. An image of the base of the pendulum of the real-life setup is presented in Appendix D.

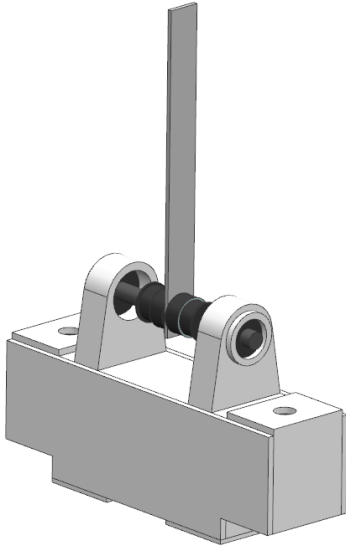


Figure 5.6: Visualization of base of pendulum

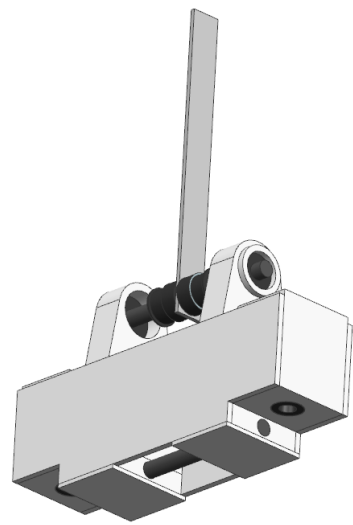


Figure 5.7: Visualization of base of pendulum

### 5.3 Design evaluation

#### Stabilization of the pendulum

The self-made test setup is able to stabilize pendulums with different lengths. The pendulums used in this setup are aluminum strip-profiles. The setup is unable to stabilize the pendulum with a length of 5 [cm], but the pendulums with a length in the range of 7.5 - 30 [cm] can be stabilized.

#### Manufacturability

An important feature of the design is that it should be affordable and easy to manufacture. The DC-motor has been obtained from an old mail sorting machine, and was therefore free. Most of the components that were used were already available, or they can either be bought in an arbitrary DIY-store or on online-webstores. The parts of the assembly in this report that were not already available are bought at tinytronics [6] for a relatively low price. The 3D-printed parts can be printed at the university (for free) or with a simple commercially available 3D-printer.

#### Oscillation of pivot point

One of the most important features of the design is the vertical oscillation of the pivot point. The horizontal position of the pivot point of the pendulum is described by the theoretical oscillation, presented below. In this expression,  $a$  represents the amplitude of the oscillation,  $b$  represents the length of the connecting rod and  $\omega$  represents the angular velocity of the flywheel.

$$y_{theoretical}(t) = -a \cdot \cos(\omega t) + \sqrt{b^2 - a^2 \cdot \sin^2(\omega t)} \quad (5.1)$$

There are several reasons as to why this oscillation could be disturbed. For instance, the weight of the pendulum-base could cause the acceleration downwards to be significantly higher than the acceleration upwards. Furthermore, some of the energy of the oscillation could be absorbed by vibrations of the test-setup. To validate whether this is the case, the vertical position of the pendulum-base is measured as a function of time. This oscillation is then compared to the theoretical oscillation and simplified oscillation. The position is measured using the technique elaborated in Appendix B, with a frame rate of 120 [FPS]. The result is presented in the figure below. The theoretical oscillation is very similar to the measured oscillation, meaning that the test setup works properly. Furthermore, the oscillation profile is also similar to the simplified oscillation profile, used in the numerical model that computes the stability.

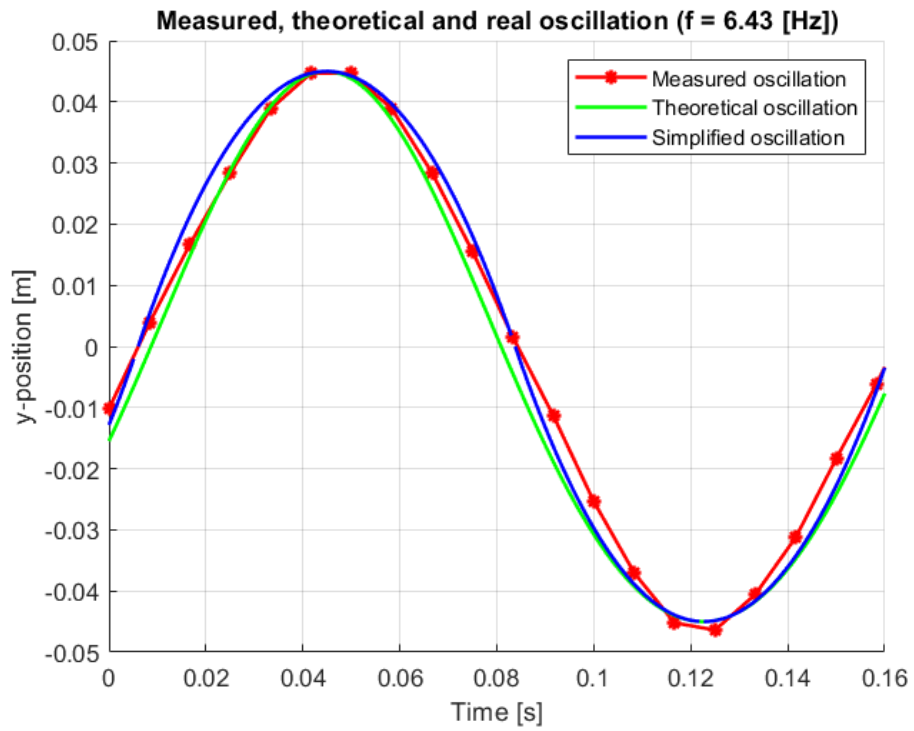


Figure 5.8: Comparison of measured, theoretical and simplified oscillation for 1 period, at a frequency of  $f = 6.43$  [Hz] and measured with a framerate of 120 [FPS].

## 6 Model v.s. experiment in upper equilibrium position

In this chapter, the model that computes the stability regions around the upper equilibrium position of the pendulum is validated. This is done with a low-budget test setup elaborated in chapter 5. First, it is explained how the experiment is conducted. Then, the assumptions w.r.t. the pendulum used in the experiment are elaborated. Finally, the experimental results are compared with the predictions of the model to determine its accuracy.

### 6.1 Explanation of experiment

The figure below shows a schematic representation of the test setup used to validate the upper equilibrium position stability regions. As explained in chapter 5, the base (and therefore also the pivot point) of the pendulum is oscillated by rotating the crankshaft with radius  $a = 45$  [mm]. The crankshaft and base of the pendulum are connected by a connecting rod with length  $b = 300$  [mm]. The damping coefficient of the pivot point is  $d = 0.0025$  [Ns/m]. The estimation of this damping coefficient is presented in Appendix A. The angular velocity of the crankshaft (and therefore also the excitation frequency) can be varied using a motor driver that controls the speed of the DC-motor. In the experiment, the pendulum is initially pointed up. When the pivot point is oscillating, the pendulum is released, and it is observed whether the pendulum keeps pointing upwards or falls down, i.e. whether the system is stable or unstable. This is done for varying excitation frequencies and lengths of the pendulum. The stability regions are documented. Because the base of the pendulum is oscillating too fast to determine its frequency by eye, a video is made of the experiment. This video is imported into a MATLAB-script that determines its frequency. The method for this frequency estimation is presented in Appendix B.

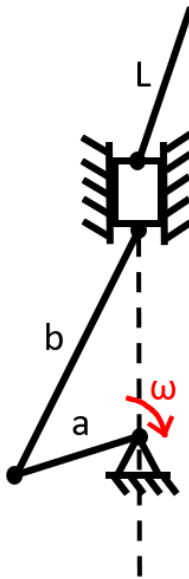


Figure 6.1: Sketch of pendulum-problem of the setup for stabilization of upper equilibrium position

### 6.2 Assumptions for the predicted stability regions

The figure below shows a schematic representation of the pendulum and axis that are used in the experiment.  $G_{axis}$  and  $G_{pendulum}$  represent the center of mass of the pendulum and axis respectively, and  $G$  represents the center of mass of the axis and pendulum combined. As presented in Figure 5.6 and Figure 5.7, the pendulum is attached rigidly to this axis around which it rotates. Therefore, for relatively short pendulums, the mass and mass moment of inertia of the axis have to be taken into account for the stability analysis, as well as the distance  $\Delta L$ . For longer pendulums, these quantities can be neglected, and the expressions of the system parameters are simplified.

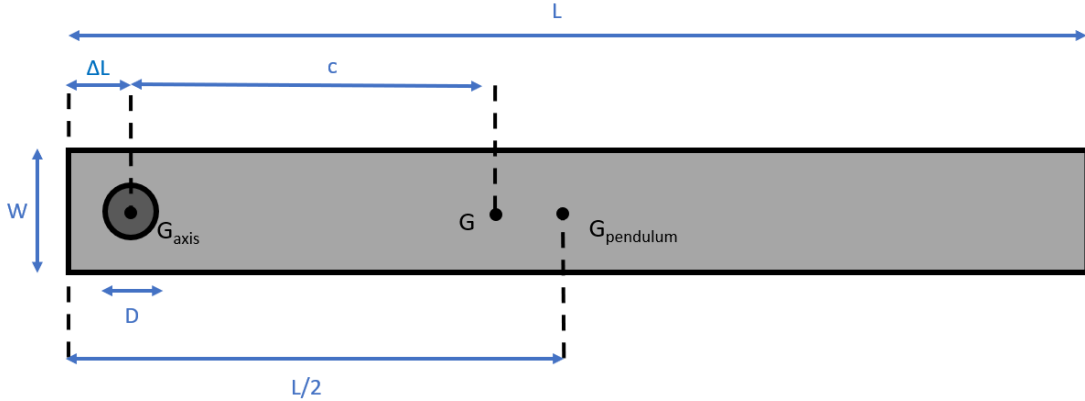


Figure 6.2: Schematic representation of the pendulum with dimensions.  $D = 8$  [mm],  $W = 15$  [mm] and  $\Delta L = 10$  [mm].

### Stability analysis for long pendulums

For long pendulums,  $\Delta L$  can be neglected w.r.t. the length of the pendulum  $L$  when determining distance  $c$ , as shown below.

$$c = \frac{1}{2}L - \Delta L \xrightarrow{\Delta L \ll L} c \cong \frac{1}{2}L \quad (6.1)$$

Furthermore, the mass moment of inertia of the axis is neglected w.r.t. the mass moment of inertia of the pendulum. The resulting expression for the inertia is given below.

$$I_G = \frac{1}{12}mL^2 \quad (6.2)$$

When this is filled into the 3 system parameters, it becomes clear that both  $\varepsilon$  and  $\omega$  are independent of the mass of the pendulum.

$$\varepsilon = \frac{m \cdot c \cdot \ddot{y}}{mc^2 + I_G} = \frac{c \cdot \ddot{y}}{c^2 + \frac{1}{12}L^2} \xrightarrow{c \cong \frac{1}{2}L} \varepsilon = \frac{3\ddot{y}}{2L} \quad (6.3)$$

$$\omega^2 = \frac{m \cdot c \cdot g}{mc^2 + I_G} = \frac{c \cdot g}{c^2 + \frac{1}{12}L^2} \xrightarrow{c \cong \frac{1}{2}L} \omega^2 = \frac{3g}{2L} \quad (6.4)$$

$$\beta = \frac{d}{mc^2 + I_G} = \frac{d}{mc^2 + \frac{1}{12}mL^2} \xrightarrow{c \cong \frac{1}{2}L} \beta = \frac{3d}{mL^2} \quad (6.5)$$

### Stability analysis for short pendulums

For short pendulums,  $\Delta L$  and the mass moment of inertia of the axis cannot be neglected. The expression for the distance from the center of mass to the pivot point ( $c$ ) and the mass moment of inertia around the

total center of mass G ( $I_G$ ) are presented below. These expressions can be directly filled into the 3 system parameters  $\varepsilon$ ,  $\omega$  and  $\beta$  to analyze the stability.

$$c = \frac{m_{axis} \cdot dL + \frac{1}{2} \cdot m_{pend} \cdot L}{m_{axis} + m_{pend}} - dL \quad (6.6)$$

$$I_G = \frac{1}{2} \cdot m_{axis} \cdot r_{axis}^2 + m_{axis} \cdot c^2 + \frac{1}{12} \cdot m_{pend} \cdot L^2 + m_{pend} \cdot \left(\frac{1}{2}L - dL - c\right)^2 \quad (6.7)$$

### 6.3 Model vs. experiment comparison

The 2 figures below show the length of the eigenvectors of the system around the upper equilibrium position. For the sake of accuracy, this is done without neglecting  $\Delta L$  and the inertia of the axis, i.e. with the assumption of short pendulums.

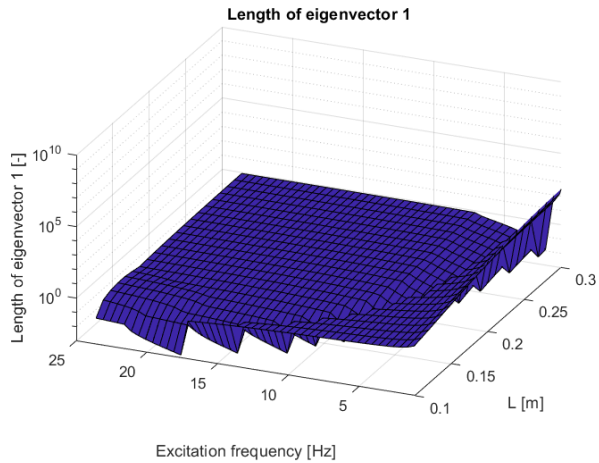


Figure 6.3: Length of eigenvector 1

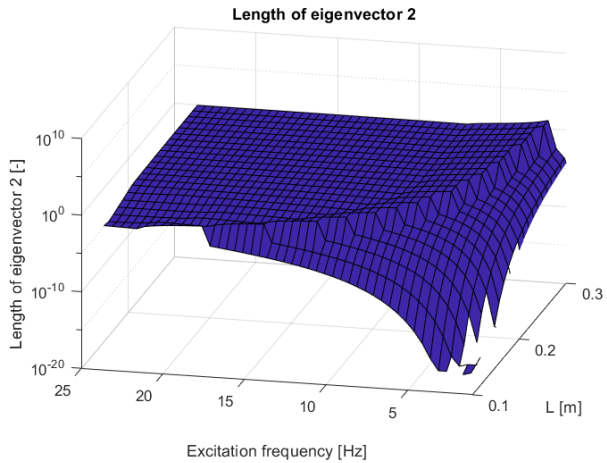


Figure 6.4: Length of eigenvector 2

Figure 6.5 shows the predicted and measured instability regions as a function of the excitation frequency and length of the pendulum. The predicted instability region is based on the length of the eigenvectors in Figure 6.3 and Figure 6.4. The results are also compared in the table below.

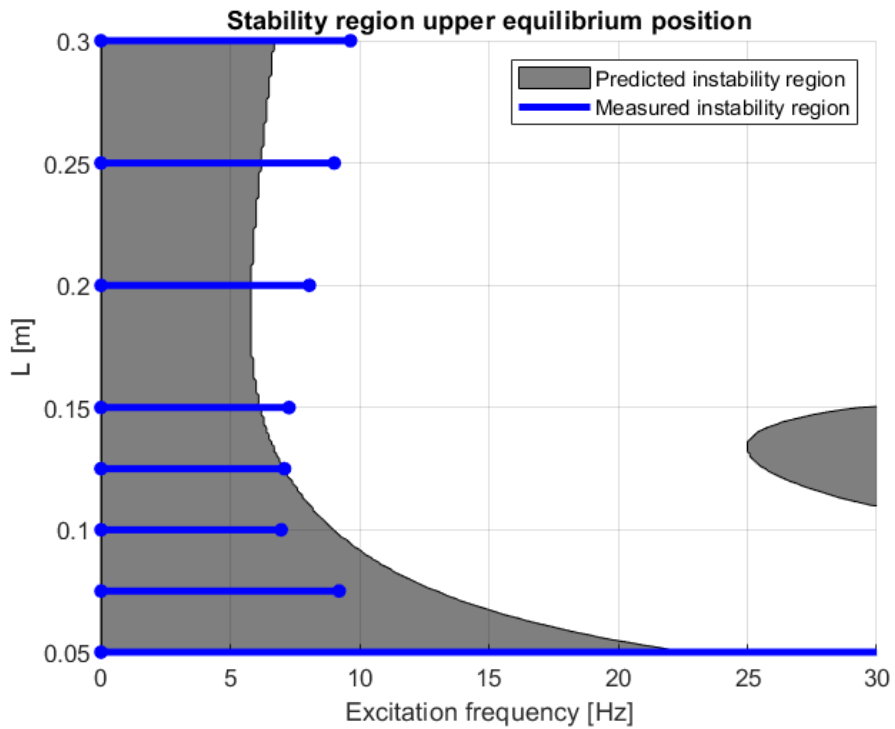


Figure 6.5: Comparison of predicted and measured instability regions around upper equilibrium position

Length L [cm]	Measured instability region [Hz]	Predicted instability region [Hz]
5	0 - unknown	0 - 22.7
7.5	0 - 9.21	0 - 13.0
10	0 - 6.97	0 - 9.0
12.5	0 - 7.1	0 - 7.1
15	0 - 7.27	0 - 6.2
20	0 - 8.06	0 - 5.09
25	0 - 9.02	0 - 6.4
30	0 - 9.65	0 - 7.7

Table 6.1: Comparison of predicted and measured instability regions around upper equilibrium position, without the extra instability region on the right side of Figure 6.5

Qualitatively, the model predicts the behaviour of the experiment relatively well. Both the model and experiment show that really short pendulums are really hard to stabilize, i.e. a high excitation frequency is required to get out of the (grey) instability region. When the length of the pendulum is increased, this required excitation frequency decreases. However, when the length is increased even further, this required excitation frequencies increases again. This quantitative behaviour, i.e. the general shape of the stability region, are similar for the model and experiment. Figure 6.5 shows that there is a new instability zone on the right part of the plot, for lengths between 10 and 15 [cm] and frequencies above 25 [Hz]. However, this region is never reached in the experiment.

Quantitatively, there is an inaccuracy between the model and the experiment. For pendulums with a length of 15 [cm] or higher, the predicted excitation frequency required to stabilize the pendulum is lower than the measured frequency in the experiment. For pendulums with a length of 10 [cm] or lower, the predicted excitation frequency required to stabilize the pendulum is higher than the measured frequency in the experiment. The model predicts the behaviour of pendulums with lengths between 10 and 15 [cm] relatively well.

For a pendulum with a length  $l = 5$  [cm], the model predicts an excitation frequency of 22.7 [Hz] is required. However, the setup is unable to stabilize this pendulum within the range of frequencies. Therefore, it is concluded that the model qualitatively predicts the behaviour of the experiment, but with a quantitative inaccuracy.

#### 6.4 Possible causes for model inaccuracy

As mentioned, there is a quantitative inaccuracy between the instability region predicted by the model and the measured instability region. A possible cause for this could be the fact that the simplified oscillation profile used in the model is not similar enough to the actual oscillation profile of the test setup. The oscillation profiles are compared in Figure 5.8. During the experiments, it is also noticed that for excitation frequencies just outside the instability region, the pendulum stabilizes but with a slight tilt towards the right side. This tilt is independent on the direction of rotation of the crankshaft and on the orientation of the pendulum on the axis. The tilt is larger for larger pendulums, and disappears when the frequency is increased, i.e. when the system moves further away from the instability region. This could be caused by imperfections of the manufactured pendulums or by vibrations of the entire test setup.

### 7 Conclusion

The main goal of this project is to design and build a simple experimental setup to stabilize a pendulum in the upper equilibrium position, and to develop a model that describes the behaviour of the pendulum in this experimental setup. The experimental setup has been made with relatively cheap products and is assembled by hand without any complicated proceedings. It can stabilize pendulums in the upper equilibrium positions for different lengths. The numerical model predicts the stability behaviour of the pendulum around its lower equilibrium position accurately. The model is also able to qualitatively predict the stability behaviour of the pendulum around the upper equilibrium position. Quantitatively, there is an inaccuracy between the model and the experiment around the upper equilibrium position. Furthermore, data has been successfully obtained from the experiments using remote measurement techniques, by making a video and analyzing this video afterwards with a MATLAB-script.

## References

- [1] A. Maki, L. Virgin, N. Umeda, T. Ueta, Y. Miino, M. Sakai, and H. Kawakami, “On the loss of stability of periodic oscillations and its relevance to ship capsizing,” *Journal of Marine Science and Technology (Japan)*, vol. 24, no. 3, pp. 846–854, 2019.
- [2] “bridge - Tacoma Narrows — Britannica.” [Online]. Available: <https://www.britannica.com/technology/bridge-engineering/Tacoma-Narrows>
- [3] A. Pogromsky and J. E. Rooda, “Modeling and Control of Manufacturing Networks . Part I,” 2008.
- [4] A. Pogromsky, “4DM40 — Modeling and Control of Manufacturing Networks,” vol. 3, pp. 7–8, 2019.
- [5] “GR 63X25, 24V - GR/G — DC Motoren - Dunkermotoren GmbH.” [Online]. Available: <https://www.dunkermotoren.de/produkte/gleichstrommotoren/detail/8844201221/>
- [6] “TinyTronics: Electronics for a tiny price!” [Online]. Available: <https://www.tinytronics.nl/shop/nl>

## Appendices

### A Appendix: Estimation of damping coefficients

In this chapter, it is explained how the damping coefficients of the test setup provided by the TU/e and the self-made setup are estimated. Note that for both setups, a viscous frictional force is assumed, meaning that the magnitude of the force is linearly proportional to the angular velocity of the pendulum.

#### A.1 Estimation of damping coefficient TU/e setup

To determine the damping constant of the TU/e setup, a simple experiment is executed, where the pendulum oscillates around its lower equilibrium position without any excitation of the pivot point. The experiment is conducted with a pendulum with a length of  $L = 68$  [cm] and a mass of  $m = 124$  [g]. A video is made of the pendulum, to measure the angle  $\phi$  w.r.t. the vertical as a function of time. It is assumed that the amplitude of the oscillation decreases according to Equation A.1. Therefore, 2 functions are fitted through the minima and maxima of  $\phi$ . Figure A.1 shows the measured  $\phi$ , together with the lines plotted through the maxima and the minima of  $\phi$  and the fitted functions through these maxima and minima. The measurement technique for this angle  $\phi$  is elaborated in Appendix B.

$$\kappa_1(t) = C \cdot e^{-\xi \cdot t} \quad (\text{A.1})$$

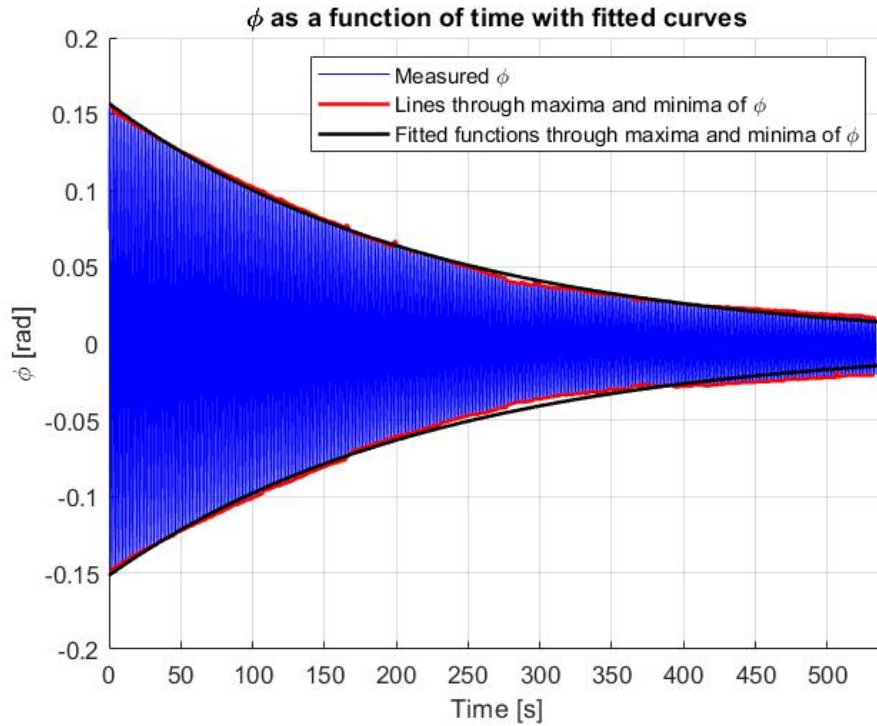


Figure A.1: Measured  $\phi$ , together with the lines plotted through the maxima and the minima of  $\phi$  and the fitted functions through these maxima and minima

The expressions of the fitted functions through the minima and maxima are presented in Equation A.2 and Equation A.3.

$$\kappa_1(t) = 0.1272 \cdot e^{-0.004479 \cdot t} \quad (\text{A.2})$$

$$\kappa_2(t) = -0.1252 \cdot e^{-0.004376 \cdot t} \quad (\text{A.3})$$

If the Lagrangian differential equation is applied to the TU/e setup, Equation A.4 is obtained. This equation is linearized around  $\phi = 180^\circ$ , and a new variable  $\psi$  is introduced. The linearized differential equation is presented in Equation A.5.

$$mL^2 \cdot \ddot{\phi} + d \cdot \dot{\phi} - mLg \cdot \sin(\phi) = 0 \quad (\text{A.4}) \quad mL^2 \cdot \ddot{\psi} + d \cdot \dot{\psi} + mLg \cdot \psi = 0 \quad (\text{A.5})$$

Equation A.5 is divided by  $mL^2$  to obtain Equation A.6. It is interesting to notice that in this form,  $\dot{\psi}$  and  $\psi$  are multiplied by  $\beta$  and  $\omega^2$  respectively. In dynamics, this form of a differential equation represents a simple mass-spring-damper system, as presented in Equation A.8. Note that this is only an approximation, as the actual system of Equation A.4 is non-linear due to the term  $\sin(\phi)$ .

$$\ddot{\psi} + \frac{d}{mL^2} \cdot \dot{\psi} + \frac{g}{L} \cdot \psi = 0 \quad (\text{A.6}) \quad \ddot{\psi} + \beta \cdot \dot{\psi} + \omega^2 \cdot \psi = 0 \quad (\text{A.7})$$

$$\ddot{\psi} + 2\xi\omega_n \cdot \dot{\psi} + \omega_n^2 \cdot \psi = 0 \quad (\text{A.8})$$

This means that the eigenfrequency of the pendulum is given by Equation A.9. To verify the equation, the eigenfrequency is calculated and compared to the measured eigenfrequency of  $\omega_n = 3.800$  [rad/s]. The 2 values are indeed close to each other, and therefore the equation is deemed to be correct.

$$\omega_n = \sqrt{\frac{g}{L}} = \sqrt{\frac{9.81}{0.68}} = 3.798 \text{ [rad/s]} \quad (\text{A.9})$$

Using this expression for  $\omega_n$ , the damping coefficient  $d$  can be calculated, as presented in Equation A.10.

$$\frac{d}{mL^2} = 2 \cdot \xi \cdot \omega_n \rightarrow d = 2 \cdot mL^2 \cdot \omega_n \cdot \xi \quad (\text{A.10})$$

If the values of the experimental pendulum are filled in,  $d_1$  and  $d_2$  are obtained from the maxima and minima respectively.

$$d_1 = 0.0020 \quad (\text{A.11}) \quad d_2 = 0.0020 \quad (\text{A.12})$$

## A.2 Estimation of damping coefficient self-made setup

To determine the damping constant of the self-made setup designed to stabilize the upper equilibrium position, a video is made where the pendulum oscillates around its lower equilibrium position due to an initial angular offset. The experiment is conducted with a pendulum of  $L = 35$  [cm],  $c \cong L$  and  $m = 24$  [g]. The angle of the pendulum w.r.t. the vertical  $\phi$  is measured as a function of time. It is assumed that the amplitude of the oscillation decreases according to Equation A.13. 2 functions are fitted through the maxima and minima, given in Equation A.14 and Equation A.15 respectively. The angle  $\phi$  together with the fitted functions through the peaks are presented in Figure B.15. The measurement technique for this angle  $\phi$  is elaborated in Appendix B.

$$\kappa(t) = C \cdot e^{-\xi \cdot t} \quad (\text{A.13})$$

$$\kappa_1(t) = 0.9087 \cdot e^{-0.2307 \cdot t} \quad (\text{A.14}) \quad \kappa_2(t) = -0.8789 \cdot e^{-0.2479 \cdot t} \quad (\text{A.15})$$

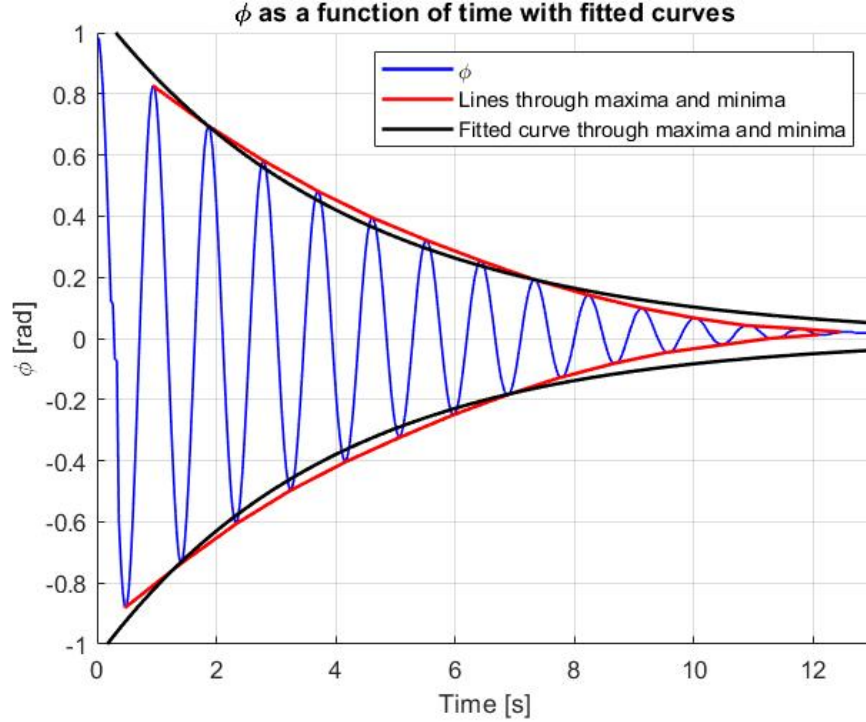


Figure A.2: Measured angle  $\phi$  as a function of time, with lines and fitted functions through maxima and minima

If the Lagrangian differential equation is applied to the test setup, Equation A.16 is obtained. This equation is linearized around  $\phi = 180^\circ$ , and a new variable  $\psi$  is introduced. The linearized differential equation is presented in Equation A.17.

$$\frac{1}{3}mL^2 \cdot \ddot{\phi} + d \cdot \dot{\phi} - \frac{1}{2}mLg \cdot \sin(\phi) = 0 \quad (\text{A.16}) \quad \frac{1}{3}mL^2 \cdot \ddot{\psi} + d \cdot \dot{\psi} + \frac{1}{2}mLg \cdot \psi = 0 \quad (\text{A.17})$$

Equation A.17 is divided by the  $\frac{1}{3}mL^2$  to obtain Equation A.18. It is interesting to notice that in this form,  $\dot{\psi}$  and  $\ddot{\psi}$  are multiplied by  $\beta$  and  $\omega^2$  respectively. In dynamics, this form of a differential equation represents a simple mass-spring-damper system, as presented in Equation A.20.

$$\ddot{\psi} + \frac{3d}{mL^2} \cdot \dot{\psi} + \frac{3g}{2L} \cdot \psi = 0 \quad (\text{A.18}) \quad \ddot{\psi} + \beta \cdot \dot{\psi} + \omega^2 \cdot \psi = 0 \quad (\text{A.19})$$

$$\ddot{\psi} + 2\xi\omega_n \cdot \dot{\psi} + \omega_n^2 \cdot \psi = 0 \quad (\text{A.20})$$

This means that the eigenfrequency of the pendulum is given by Equation A.21. To verify the equation, the eigenfrequency is calculated and compared to the measured eigenfrequency of  $\omega_n = 6.958$  [rad/s]. The 2

values are indeed close to each other, and therefore the equation is deemed to be correct.

$$\omega_n = \sqrt{\frac{3g}{2L}} = \sqrt{\frac{3 \cdot 9.81}{2 \cdot 0.305}} = 6.946 \text{ [rad/s]} \quad (\text{A.21})$$

Using this expression for  $\omega_n$ , the damping coefficient d can be calculated, as presented in Equation A.22.

$$\frac{3d}{mL^2} = 2 \cdot \xi \cdot \omega_n \rightarrow d = \frac{2}{3} \cdot mL^2 \cdot \omega_n \cdot \xi \quad (\text{A.22})$$

If the values of the experimental pendulum are filled in,  $d_1$  and  $d_2$  are obtained from the maxima and minima respectively.

$$d_1 = 0.0024 \quad (\text{A.23}) \quad d_2 = 0.0026 \quad (\text{A.24}) \quad d_{\text{average}} = 0.0025 \quad (\text{A.25})$$

## B Appendix: Measurement technique with video

### B.1 Error of video

To determine the damping constant for both test setups, the angle of the pendulum as a function of time is measured. This is done by placing a camera in front of the pendulum, perpendicular to the plane in which the pendulum oscillates. The front view of Figure B.1 shows the pendulum from the point of view from the camera. The top view shows a schematic representation of the camera placement w.r.t. the pendulum.  $u$  represents the horizontal deflection of the tip of the pendulum.  $\theta$  represents the angle of the pendulum w.r.t. the vertical. The displacement of the tip of the pendulum is measured using a reference wall with a known length.  $i$  and  $j$  represent the distance between the camera and pendulum-tip, and the distance between the pendulum-tip and reference wall respectively.

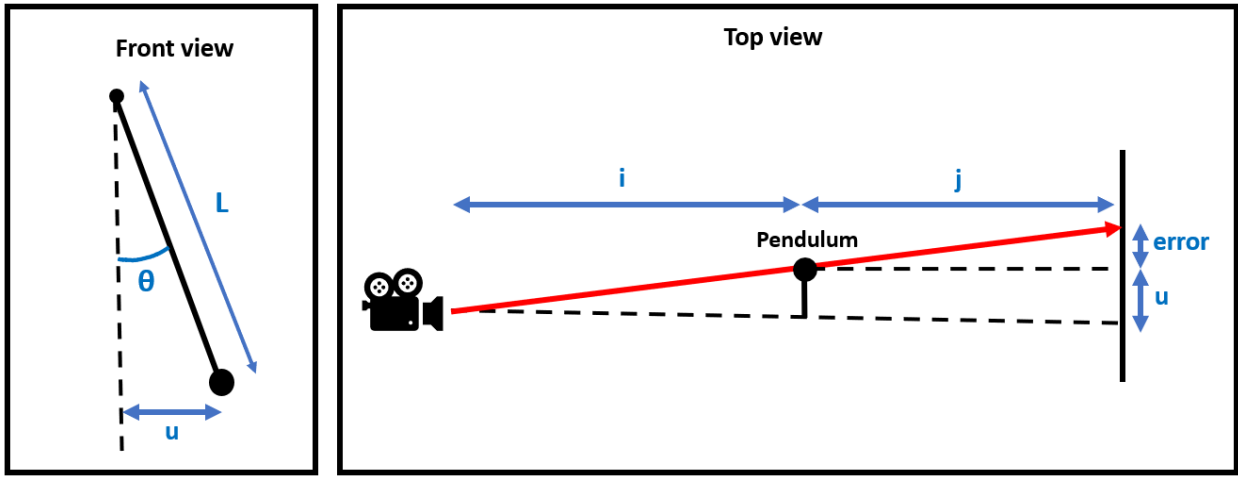


Figure B.1: Top view

Figure B.1 shows that if  $j \neq 0$ , there is an inaccuracy between the measured horizontal displacement of the pendulum-tip and the actual horizontal deflection. This inaccuracy is characterized by the error. Equation B.1 shows that the magnitude of this error is linearly proportional to ratio  $\frac{j}{i}$ , i.e. in order to minimize this error,  $\frac{j}{i}$  should be as small as possible. In practice, this means that the camera should be placed far from the pendulum, and the pendulum should be placed as close to the reference wall as possible. Note that, as  $j \geq 0$ , the measured angle displacement is always larger than the actual angle, and the error cannot be negative.

$$\text{error} = u \cdot \frac{i+j}{i} - u = u \cdot \frac{j}{i} \quad (\text{B.1})$$

The angle of the pendulum w.r.t. the horizontal is computed using its the horizontal displacement  $u$  and the pendulum length  $L$ . Equation B.2 shows the expression for the actual angle  $\theta$ , and Equation B.3 shows the expression for the measured angle  $\theta$ .

$$\theta_{\text{real}} = \arcsin\left(\frac{u}{L}\right) \quad (\text{B.2}) \quad \theta_{\text{measured}} = \arcsin\left(\frac{u + \text{error}}{L}\right) = \arcsin\left(\frac{u \cdot \left(\frac{j}{i} + 1\right)}{L}\right) \quad (\text{B.3})$$

To determine whether this error in angle is significant, the difference in angles is plotted as a function of the horizontal displacement  $u$  in Figure B.2. This is done with the values of  $\frac{j}{i}$  and  $L$  that were used for the damping coefficient measurements. The figure shows that the difference in angle becomes larger for larger

deflections  $u$ . Furthermore, the maximum difference in angle is  $0.32 [{}^\circ]$ . As the stability computations do not have a big dependency of the damping coefficient, and the difference in angle is relatively small, this effect is neglected for the angle computation.

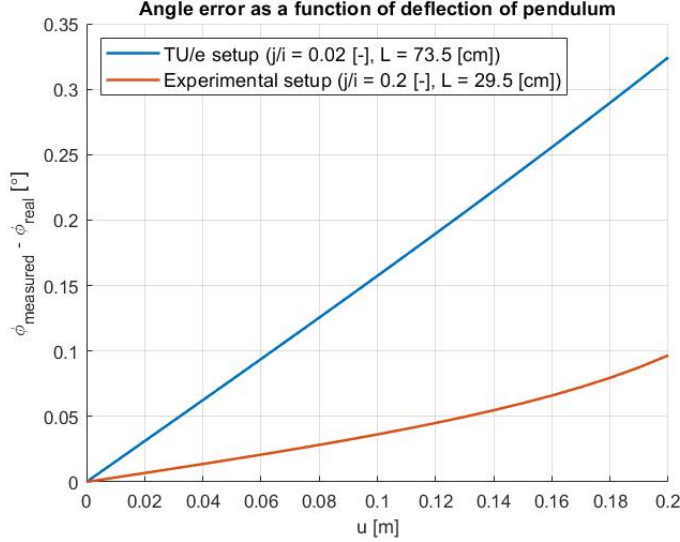


Figure B.2: Top view

## B.2 Explanation of position extraction from video

In this section, it is explained how the position of a certain object is obtained from frames of a video. First, the video is imported into the MATLAB-workspace using the **VideoReader()** command. The MATLAB-script that is used for this is presented in subsection E.2. Next, the frames of the video are read separately using the **readFrame()** command. This command imports the frame of the video as 3 2D-matrices, where each element of the matrix represent a pixel. The 3 matrices contain the RGB-value of each pixel. Figure B.3 shows a schematic representation of an image as pixels. In this case, the amount of pixels in the x-direction of the image  $W_{\text{pix}} = 12$  [pixels] and the amount of pixels in the y-direction of the image  $H_{\text{pix}} = 6$  [pixels]. The figure also shows the method of indexing of the pixels, starting from the top left corner.

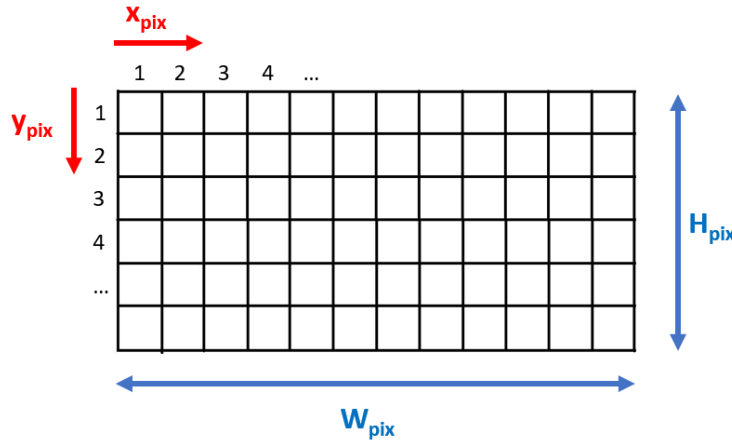


Figure B.3: Explanatory representation of image as pixels;  $W_{\text{pix}} = 12$  [pixels] and  $H_{\text{pix}} = 6$  [pixels]

Using 2 for-loops (1 for each dimension of the matrix), all pixels of the matrix are evaluated. If the values

satisfy a certain pre-defined condition considering the RGB-value of pixels, the location of the pixel is saved. The RGB-value of a pixel represents the red-blue-green value of a pixel. Each pixel is characterized by 3 numbers, each number varying from 0 to 255. This means that there are  $256^3$  possible possibilities for each pixel. After finishing the 2 for-loops, the median of the pixels is taken to obtain the center of the desired object in the video, denoted by  $\bar{r}_{rel} = [x_{rel} \ y_{rel}]^T$ . Note that these are indexes of the selected pixel. To convert this to the actual position of the object (in meters), Equation B.4 and Equation B.5 are used. Here, H and W are the height and width of the reference wall in the frame respectively, and the reference system is placed in the bottom left corner of the image.

$$x_{rel} = \frac{x_{pix}}{W_{pix}} \rightarrow x = x_{rel} \cdot W \quad (B.4) \quad y_{rel} = 1 - \frac{y_{pix}}{H_{pix}} \rightarrow y = y_{rel} \cdot H \quad (B.5)$$

To determine the pre-defined condition for the RGB-values, the 3 matrices obtained from the **readFrame()** are plotted separately, meaning that the 3 plots represent the R-, G- and B-value respectively. In these plots, it is clearly visible that the desired objects have distinct RGB-values. Based on these plots, the conditions regarding the RGB-values are determined. In the following 3 sections, a selected original frame from a video is depicted, together with the frame where the selected pixels are colored red and the middle of the selected pixels is marked green. Furthermore, the R-, G- and B-value are plotted for the original frame. This is done for a video that was used to determine the excitation frequency of the experiment with the self-made setup, for the video that was used to estimate the damping coefficient of the self-made setup and for the video that was used to estimate the damping coefficient of the setup provided by the TU/e.

### B.2.1 Frequency estimation of self-made setup

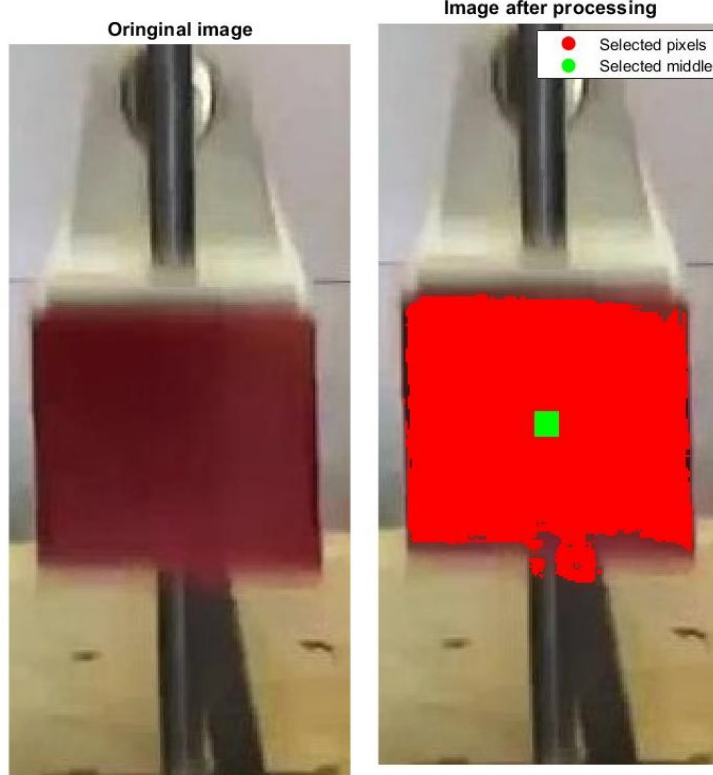


Figure B.4: Original frame from video; fps = 120 [frames/s], zoomed in on the base of the pendulum  
 Figure B.5: Analyzed frame; selected pixels (that satisfy the RGB-condition) are marked red, the selected middle 10x10 pixels is marked green

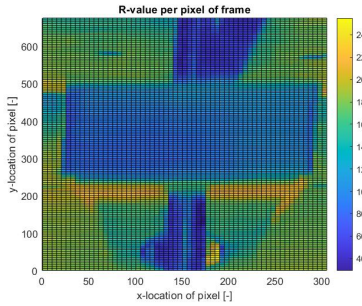


Figure B.6: R-value

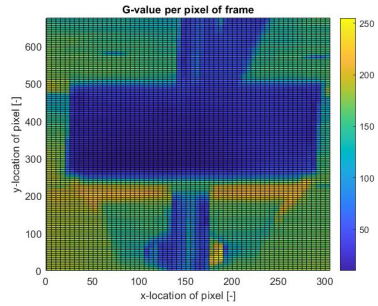


Figure B.7: G-value

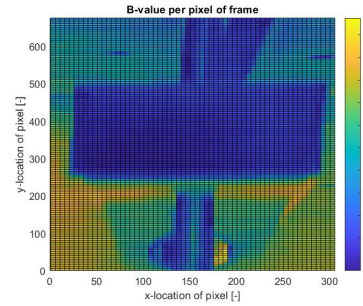


Figure B.8: B-value

### B.2.2 Damping estimation of self-made setup

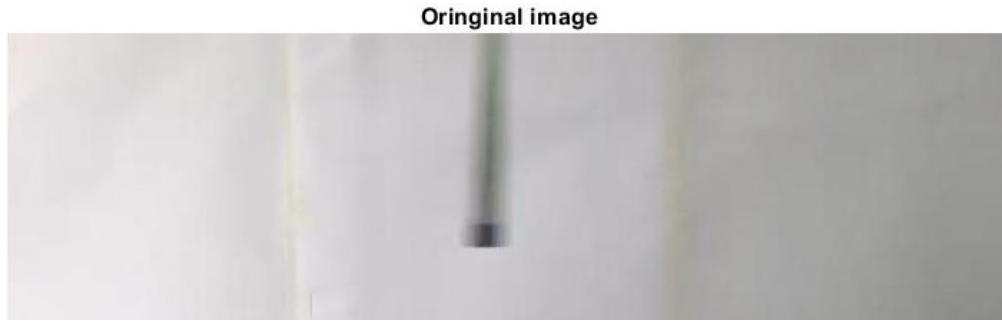


Figure B.9: Original frame from video; fps = 120 [frames/s]

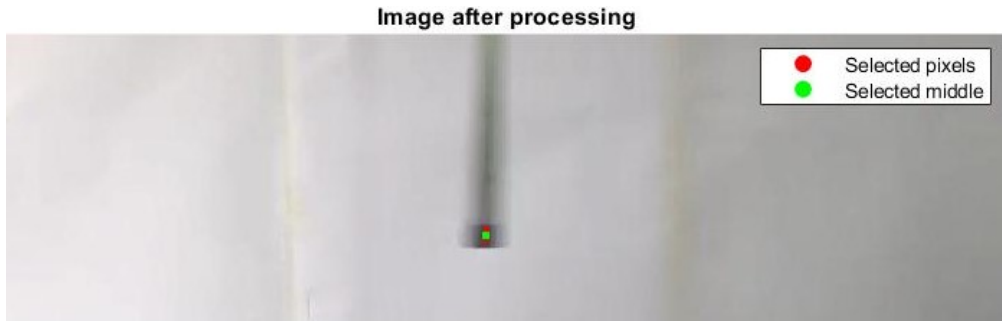


Figure B.10: Analyzed frame; selected pixels (that satisfy the RGB-condition) are marked red, the selected middle 5x5 pixels is marked green

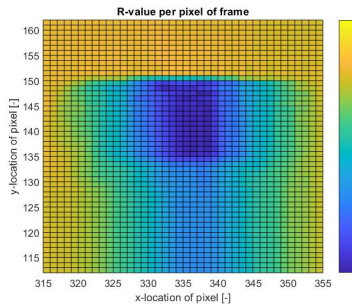


Figure B.11: R-value

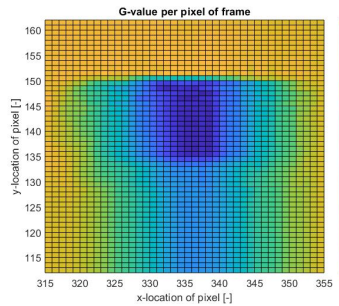


Figure B.12: G-value

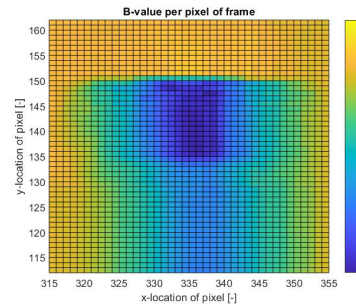


Figure B.13: B-value

### B.2.3 Damping estimation of TU/e setup

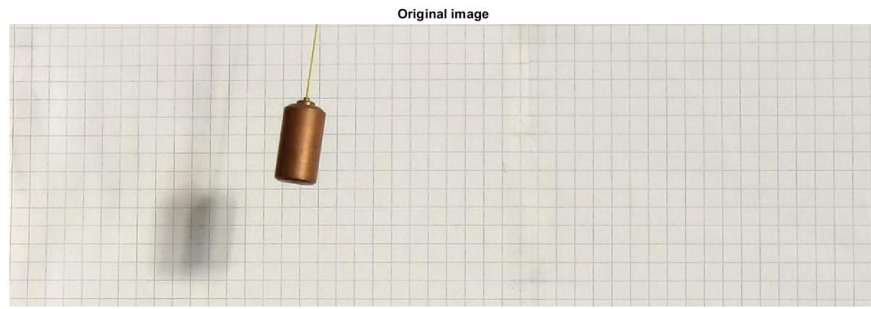


Figure B.14: Original frame from video; fps = 120 [frames/s]

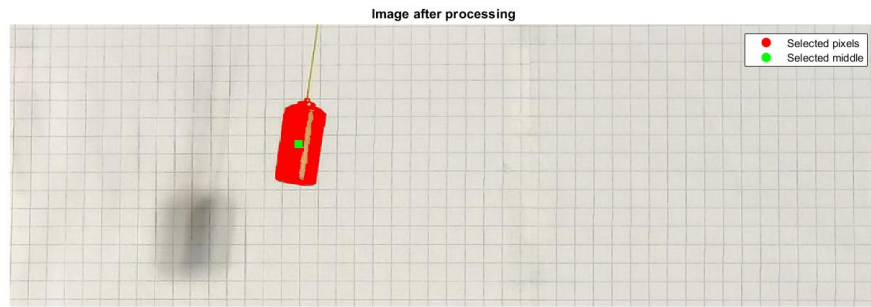


Figure B.15: Analyzed frame; selected pixels (that satisfy the RGB-condition) are marked red, the selected middle 10x10 pixels is marked green

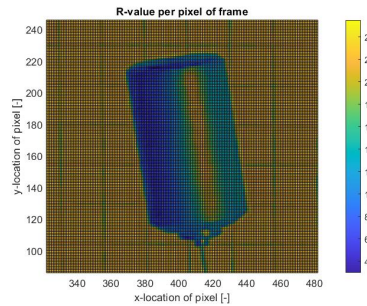


Figure B.16: R-value

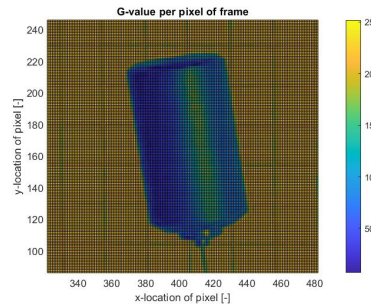


Figure B.17: G-value

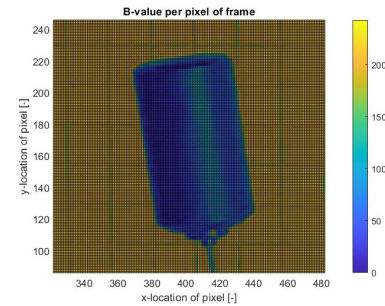


Figure B.18: B-value

## C Appendix: Data sheet of DC-motor

**» GR 63x25 | cont. 50 W, peak 119 W**

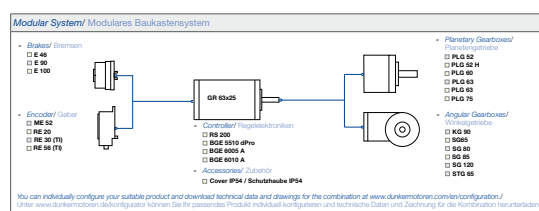
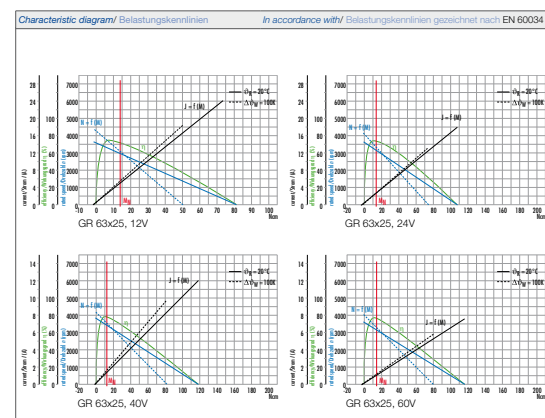
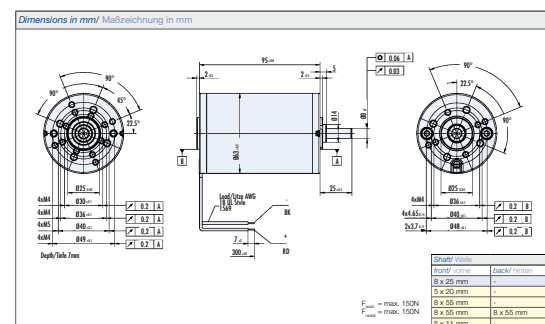
• Operation in both directions of rotation  
• Ball bearing at motor output shaft is standard  
• With custom shaft length and diameter,  
shaft on both sides, special and high voltage  
winding, higher protection class up to IP 67,  
reinforced bearing on request

• Drehrichtung Rechts-/ Linkslauf  
• Motorentriebwellenlager ist Standard  
• Abweichende Wellenlängen - durchmesser,  
bedienter Seite, Sonder- und Hochspannungs-  
wicklungen, höheres Schutzart bis IP 67, verstärkte  
Lagerung auf Anfrage

Data/ Technische Daten		GR 63x25			
Nominal voltage/ Nominal current	VDC	12	24	40	60
Nominal current/ Nominal torque	A <sup>1</sup>	5.2	2.7	1.65	1.1
Nominal speed/ Nominal power	Nm <sup>1</sup>	0.137	0.14	0.133	0.145
Shaft torque/ Antriebsmoment	Nm <sup>1</sup>	1.05	1.08	1.18	1.16
Maximum torque/ Maximales Antriebsmoment	Nm <sup>1</sup>	1.05	1.08	1.18	1.16
No load speed/ Leeraufdrehzahl	rpm <sup>1</sup>	3600	3600	3600	3600
Nominal output power/ Nominalleistung	W <sup>1</sup>	44.5	48.4	48.7	50
Maximum output power/ Maximale Ausgangsleistung	W	99	101.8	117.4	119.3
Torque constant/ Drehmomentkonstante	Nm A <sup>-1</sup>	0.0313	0.06	0.098	0.153
Terminal Resistance/ Endspannungswiderstand	Ω	0.353	1.33	3.33	7.89
Terminal inductance/ Endspannungsspannung	mH	1	2.9	7.3	17.4
Starting current/ Anfangsstrom	A <sup>1</sup>	34	18	12	7.6
No load current/ Leeraustrittstrom	A <sup>1</sup>	0.750	0.38	0.205	0.135
Demagnetization current/ Entmagnetisierungstrom	A <sup>1</sup>	≥ 50	≥ 24	≥ 16	≥ 9.5
Rotor inertia/ Drehmassmoment	gcm <sup>2</sup>	400	400	400	400
Weight of motor/ Motorgewicht	kg	1.2	1.2	1.2	1.2

<sup>1</sup>  $\Delta \theta_a = 100 \text{ K} \cdot \text{°}$ ; <sup>2</sup>  $\theta_a = 20^\circ \text{ C}$  at nominal point / in Nennpunkt;  Preference / Vorzugsliste;  On request / auf Anfrage

**» GR 63x25 | cont. 50 W, peak 119 W**



48 | Visit [www.dunkermotoren.com](http://www.dunkermotoren.com) for further product information | Besuchen Sie [www.dunkermotoren.de](http://www.dunkermotoren.de) für weitere Produktinformationen | 48

Visit [www.dunkermotoren.com](http://www.dunkermotoren.com) for further product information | Besuchen Sie [www.dunkermotoren.de](http://www.dunkermotoren.de) für weitere Produktinformationen | 48

Figure C.1: Datasheet of DC motor used in experimental setup

## D Appendix: self-made test setup images

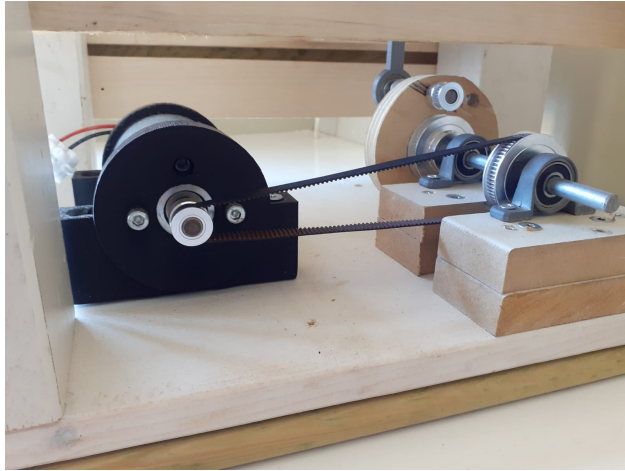


Figure D.1: Pulley system

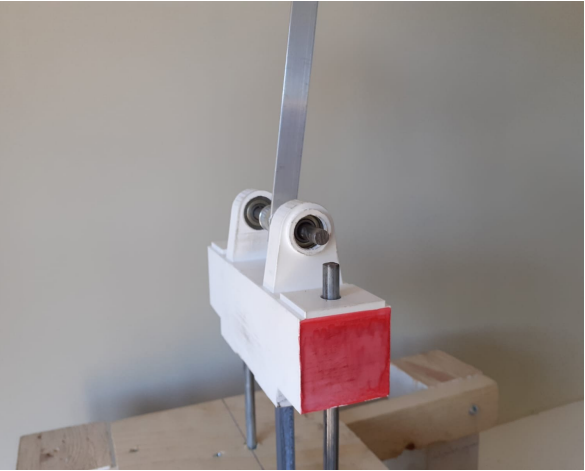


Figure D.2: Base of pendulum

## E Appendix: MATLAB-scripts

### E.1 MATLAB-script that predicts stability

```

1 clear all; close all; clc;
2 %% Code description
3 % Code that checks the stability for varying frequency and length of
4 % pendulum
5 % Computed in lower equilibrium position
6 % Store stability in matrix where 0 means a stable and 1 means unstable
7 % combination of c and f
8 %% Compute eigenvalues
9
10 % Define system parameters:
11 m = ; % Mass of pendulum
12 g = ; % Gravity constant [m/s^2]
13 I_G = ; % Mass moment of inertia [kgm^2]
14 d = ; % Damping coefficient [Ns/m] (d = 0.0024)
15 amp = ; % Amplitude of oscillation [m]
16
17 f_start = ; % Minimum excitation frequency
18 f_step = 0; % Interval of excitation frequency
19 f_end = ; % Maximum excitation frequency
20 f_array = [f_start:f_step:f_end]; % Excitation frequency array
21
22 c_start = ; % Minimum distance c
23 c_step = ; % Interval of distance c
24 c_end = ; % Maximum distance c
25 c_array = [c_start:c_step:c_end]; % Distance c array
26
27 i = 0;
28
29 for f = f_start:f_step:f_end
30
31     i = i + 1;
32
33     j = 0;
34
35     for c = c_start:c_step:c_end
36
37         j = j + 1;
38
39         T = 1/f; % Period of oscillation [s]
```

```

40     s_acc = 32*amp/(T^2); % Acceleration of oscillation [m/s^2]
41
42 % Define general system parameters:
43 omega = sqrt(m*c*g/(m*c^2+I_G));
44 eps = m*c*s_acc/(m*c^2+I_G);
45 beta = d/(m*c^2+I_G);
46
47 % Define system matrices:
48 A_1 = [0 1; -omega^2+eps -beta];
49 A_2 = [0 1; -omega^2-eps -beta];
50 M = expm(A_1*T/2) * expm(A_2*T/2);
51
52 % Find eigenvalues of matrix M:
53 e_vec = eig(M);
54
55 e_1 = e_vec(1); % eigenvector 1
56 e_2 = e_vec(2); % eigenvector 2
57
58 % Compute lengths of eigenvectors:
59 L_e_1 = sqrt(real(e_1)^2 + imag(e_1)^2);
60 L_e_2 = sqrt(real(e_2)^2 + imag(e_2)^2);
61
62 M_e_1(i,j) = L_e_1;
63 M_e_2(i,j) = L_e_2;
64
65 if L_e_1 < 1 && L_e_2 < 1 % Eigenvectors are Schur
66
67     M_stability(i,j) = 0;
68
69 else % Eigenvectors are not Schur
70
71     M_stability(i,j) = 1;
72
73 end
74
75 end
76
77 end

```

## E.2 MATLAB-script that reads video

```

1 clear all; clc;
2 %% Description of code
3 % This code imports a video of the base of the pendulum or a swinging
4 % pendulum to determine the x- and y-position as a function of time
5 % Thijs van Oorschot 1352725
6 %% Import video
7
8 v = VideoReader(''); % Import video
9 N_frames = v.NumFrames; % Import amount of frames [-]
10
11 % Code for normal video
12 FrameRate = v.FrameRate; % Import framerate of video [1/s]
13 T_video = v.Duration; % Import duration of video [s]
14 T_frame = 1 / v.FrameRate; % Time per frame [s]
15 t_array = [0:T_frame:(N_frames-1)*T_frame]; % Time array for frames [s]
16
17 H = get(v, 'Height'); % Height of frame [pixels]
18 W = get(v, 'Width'); % Width of frame [pixels]
19
20 %% Evaluate frames
21
22 i = 0;
23
24 for frame = 1:N_frames % For-loop to go through all frames
25
26     I = readFrame(v); % Read RGB-values from pixels
27
28     k = 0;
29

```

```

30     pix_x_array = zeros(1,1);
31     pix_y_array = zeros(1,1);
32
33     for h = 1:1:H
34
35         for w = 1:1:W
36
37             if I(h,w,1) > xx && I(h,w,2) < xx && I(h,w,3) < xx
38
39                 k = k + 1;
40
41                 % Save index of pixel in array
42                 pix_x_array(k) = w;
43                 pix_y_array(k) = h;
44
45         end
46
47     end
48
49 end
50
51 i = i + 1;
52
53 % Get median from obtained pixels
54 pix_x = median(pix_x_array);
55 pix_y = median(pix_y_array);
56
57 % Determine relative position in frame [-]
58 x(i) = pix_x / W;
59 y(i) = 1 - pix_y / H;
60
61 end
62
63 EQ_y = mean(y); % Find equilibrium position of pendulum-base

```